Experimental studies of antihydrogen and positronium physics: Problems and possibilities

I. N. Meshkov
Joint Institute for Nuclear Research, Dubna

Fiz. Élem. Chastits At. Yadra **28**, 495–540 (March–April 1997)

Advances in the development of methods of intense antiproton beam storing and cooling has again attracted attention to the problem of generation and experimental studies of antihydrogen atoms. An additional impetus to this activity has been given by the proof to the "existence theorem"—experiments on antihydrogen atom synthesis at CERN. The interest to antiatoms is aroused due to possibility of studies of the fundamental properties of matter, and foremost—its symmetry (the CPT theorem). This report is dedicated to description and analysis of the methods of the antiproton and positronium directed flux generation and experimental studies of the atoms in these fluxes. © *1997 American Institute of Physics.* [S1063-7796(97)00502-0]

INTRODUCTION

The physics of antihydrogen is of great interest from the viewpoint of understanding the fundamental properties of matter, and, in particular, its symmetry properties. A specific problem which was suggested by the authors of the first studies on antihydrogen production[1,2] is that of verifying the CPT theorem. This has become quite feasible since the first synthesis of antihydrogen atoms in December 1995 at the LEAR antiproton ring at CERN.[3] Alhough this experiment was essentially just a demonstration (see Sec. II A below), it can now be claimed that antihydrogen exists as a physical object.

Currently, there are two quite different approaches in antihydrogen physics. The first is the production of antihydrogen atoms one by one in antiproton and antipositron traps at ultralow energies, followed by confinement of the atoms in magnetic traps with the minimum magnetic field and cooling down to a temperature of order 1 K by means of laser radiation. Presently, most proposals for antihydrogen experiments favor this method, and it has been widely discussed in the literature (see Ref. 4 and references therein). We shall therefore not discuss it here.

The second approach is the use of antiproton and positron storage rings.[1,2] This has been under discussion for some time (see, for example, the review of Ref. 5). A variant of this idea suggested recently[6,7] would allow the production of intense pencil beams of $30-3\times10^4$ antihydrogen atoms per second with velocities in the range $0.03-0.3$ times the speed of light, respectively (antiproton energies of $0.5-50$ MeV). This setup would simultaneously produce pencil beams of orthopositronium ($30-1.7\times10^4$ sec^{-1}), which are of independent interest as an object of study.

The latter method of producing antihydrogen seems to be simpler from the viewpoint of the possibilities offered by accelerator technology. However, for a long time it has been viewed unfavorably by most experimentalists owing to the difficulties of performing experiments involving atoms of approximately relativistic velocities. There has been nearly no acknowledgement of the advantages offered by electron cooling (of both antiprotons and positrons), in particular, decrease of the spread of the atomic velocity distribution to a level $\Delta\nu/\nu\sim10^{-6}$, corresponding to a temperature of fractions of a degree Kelvin in the particle rest frame. In addition, methods of fast-atom spectroscopy are available in atomic physics (see, for example, Refs. 8–12), and a combination of these with the technique of producing cold antihydrogen atoms appears very promising.[13] The purpose of the present study is to describe the possibilities offered by experiments using beams of antihydrogen and orthopositronium.

1. PROBLEMS IN THE PHYSICS OF ANTIHYDROGEN AND POSITRONIUM

1.1. Antihydrogen and CPT invariance

The principle of CPT invariance (the CPT theorem) can be verified by comparing particle and antiparticle parameters: their masses, absolute values of the electric charges and magnetic moments, and gyromagnetic ratios. Of course, it is interesting to perform measurements at a level of accuracy exceeding that attained at present. The latter can be judged from the data of Refs. 14–16, given in Table I.

Although at present there is no experimental evidence calling the validity of CPT invariance into question, there is also no reason not to verify CPT invariance. In this respect, CPT invariance is just as much an axiom of modern physics as are other axioms. The high accuracy attained by indirect comparison of the masses of neutral kaons[17]

$$\left|\frac{m(K^0)-m(\bar{K}^0)}{m(K^0)}\right|\leqslant5\cdot10^{-19} \tag{1.1}$$

cannot serve as absolute proof of the theorem, because, in general, any particle "has the right" to be asymmetric relative to its antiparticle. Therefore, the experimental verification of the symmetry of each of the known particles is of independent importance. It is most important for the "most fundamental" particles, i.e., the proton and electron.

The use of directed fluxes of antihydrogen atoms as a test object allows direct and highly accurate comparison of the electric charges of the antiproton and positron (Sec. III). The measurement of the hyperfine structure and the Lamb shifts of the optical spectrum of antihydrogen is just as in-

 1063-7796/97/020198-18$10.00

TABLE I. Parameters of the fundamental particles.

Parameter	Value Electron and positron	Accuracy	Reference
Electron mass, MeV	0.510 099 906(15)	$3\cdot10^{-7}$	[14]
Mass difference $\lvert m^+-m^-\rvert/m^-$	$<4\cdot10^{-8}$	$<4\cdot10^{-8}$	[14]
Charge inequality $\lvert e^+-e^-\rvert/e^-$	$<4\cdot10^{-8}$	$<4\cdot10^{-8}$	[14]
Difference of the charge to mass ratios	$<3\cdot10^{-8}$	$1\cdot10^{-8}$	[14]
Electron magnetic moment (in Bohr magnetons)	1.011 159 652 193(10)	$1\cdot10^{-11}$	[14]
Gyromagnetic ratios $\lvert g^+-g^-\rvert/g^-$	$(-0.5\pm2.1)\cdot10^{-12}$	2.1×10^{-12}	[14]
	Proton and antiproton		
Proton mass, MeV	938.2723(28)	$3\cdot10^{-7}$	[14]
Mass difference, $\Delta M/M$	$<\pm4\cdot10^{-8}$	$<4\cdot10^{-8}$	[14]
Inequality of proton and electron charges, $\lvert e_p-e^-\rvert/e^-$	$<1\cdot10^{-21}$	$<1\cdot10^{-21}$	[14]
Inequality of the proton and antiproton charges, $\lvert e_p-e_a\rvert/e_p$	$<2\cdot10^{-5}$	$<2\cdot10^{-5}$	[14]
Inequality of the proton and Antiproton charge-to-mass ratios	$<1.5\cdot10^{-9}$	$<1.1\cdot10^{-9}$	[15]
Proton magnetic moment (in nuclear magnetons)	2.792 847 39(6)	$2\cdot10^{-8}$	[14]
Antiproton magnetic moment (in nuclear magnetons)	−2.8005(90)	$3\cdot10^{-3}$	[16]

teresting. As is well known, the hyperfine splitting of levels is proportional to a combination of fundamental constants (see, for example, Sec. 121 of Ref. 18):

$$\Delta\omega_{HFS}\propto\mu_p\mu_e(e_pe)^3, \tag{1.2}$$

where μ_p and μ_e are the proton (antiproton) and electron (positron) magnetic moments, and e_p and e are the proton (antiproton) and electron (positron) electric charges. Since the parameter known at present with least accuracy is μ_p (while for the antiproton this has not been measured at all), a precise measurement of $\Delta\omega_{HFS}$ would first of all allow the determination of the magnetic moment—both its absolute value and, with much higher accuracy, the relative difference between the proton and antiproton magnetic moments.

The Lamb shift is proportional to

$$\Delta\omega_L\propto me^6e_p^4, \tag{1.3}$$

where m is the electron (positron) mass. Therefore, measurement of $\Delta\omega_L$ gives information about the values of three fundamental constants [in the combination (1.3)] for particles and antiparticles.

Of course, the precise determination of $\Delta\omega_{HFS}$ and $\Delta\omega_L$ is important not only because it provides more accurate knowledge of the antiproton and positron parameters. If these values were found to differ for atoms and antiatoms, this would in itself be an indication of symmetry breaking in the fundamental interactions. In particular, the Lamb shift, which is calculated in quantum electrodynamics including radiative corrections, a parameter of the atomic spectrum-measured with a high degree of accuracy.[10] Accordingly, by comparing its values for hydrogen and antihydrogen it becomes possible to judge the symmetry of the interactions.

1.2. Positronium and QED

Positronium, being a very simple quantum system, has been described quite well theoretically and perhaps plays the same role in quantum electrodynamics as the hydrogen atom in nonrelativistic quantum mechanics.[19,20] Experiments involving positronium, which so far have been carried out under rather complicated conditions in which it is not easy to isolate the effect of the target, have, as a rule, produced rather inaccurate results, and even results which in some cases are ambiguous (Table II). A precise measurement of the positronium parameters is therefore of great interest.

1. Among experiments of this type, mention should first of all be made of the measurement of the *orthopositronium lifetime*. Its theoretical value, calculated taking into account order-α^3 radiative corrections,[21a] is

$$\tau_{\text{ortho}}^{-1}=\frac{\alpha^6mc^2}{\hbar}\cdot\frac{2(\pi^2-9)}{9\pi}\cdot\left[1-10.282(3)\frac{\alpha}{\pi}-\frac{\alpha^2}{3}\ln\alpha^{-1}+B\left(\frac{\alpha}{\pi}\right)^2-\frac{3\alpha^3}{2\pi}(\ln\alpha^{-1})^2\cdots\right], \tag{1.4}$$

where B is a numerical coefficient whose calculation is not yet complete (see Ref. 21b below). The results of experiments on the measurement of τ_{ortho} are quite contradictory (Fig. 1). The experiments performed by the Michigan group[22–24] gave a value of τ_{ortho} smaller than the theoretical value (Table II), the difference being more than 3–5 standard deviations. The Tokyo group[25] obtained a value exceeding

TABLE II. Positronium parameters.

Parameter	Theory	Experiment	Accuracy
	Orthopositronium		
Lifetime, nsec	142.08106(20) (Ref. 21a)	141.880(32) (Ref. 24)	$2\cdot10^{-4}$
	142.038 (Ref. 21b)	142.049(80) (Ref. 25)	$5\cdot10^{-4}$
Energy of $1S-2S$ transition, PHz		1.233 607 185(15) (Ref. 29)	$1\cdot10^{-8}$
	1.233 607 2355(107) (Ref. 27)	1.233 607 2189(107) (Ref. 30)	1×10^{-8}
	Agreement through α^3		
Fine structure of $2S$-$2P$ levels			
Relative probability of 2γ annihilation	0	$<1.4\times10^{-3}$ (Ref. 33)	
	Parapositronium		
Lifetime, nsec	125.16(08) (Ref. 26)	125.142 (Ref. 26)	$2\cdot10^{-4}$
Relative probability of 4γ annihilation		$<(1.3\times0.4)\cdot10^{-4}$ (Ref. 34)	
	Ground state		
Energy, eV	6.79		
Fine structure $\Delta\varepsilon_{FS}$, eV	$8.411\cdot10^{-4}$		
$\Delta\varepsilon_{FS}/2\pi\hbar$, GHz	203.4003(129) (Ref. 31)	203.38910(74) (Ref. 31)	$\pm3.6\cdot10^{-6}$

the theoretical one by about 1.5 standard deviations, which does not contradict theory,[21a,b] although the accuracy is still inadequate

2. The short *parapositronium lifetime* cannot be measured in a standard experiment. The theoretical value calculated through order α^2 is given by (see Ref. 26)

$$\tau_{\text{para}}^{-1}=\frac{\alpha^5 mc^2}{2\hbar}\left[1-\left(5-\frac{\pi^2}{4}\right)\frac{\alpha}{\pi}+\frac{2}{3}\alpha^2\ln\frac{1}{\alpha}+C\left(\frac{\alpha}{\pi}\right)^2\cdots\right]. \tag{1.5}$$

Here again the coefficient C has not been fully calculated (hence the uncertainty in the numerical value). The experimental value of τ_{para} measured[26] by the method of mixing of ortho- and parapositronium states in a magnetic field (see Sec. 6.1 below) coincides with the theoretical value (1.5) within one standard deviation.

It should be noted that the calculation of the theoretical values of τ_{ortho} and τ_{para} with accuracy $O(\alpha^2)$ is fraught with serious difficulties.[27,28] In addition to two-loop virtual corrections (not yet completely determined), it is necessary to include the comparable contribution of relativistic corrections of order $(v/c)^2$, where v is the velocity of the electron and the positron in the positronium rest frame.[27] If the theoretical values of the $O(\alpha^2)$ corrections are known, the experimental values of the relativistic corrections can be extracted from the experimental values of the o-Ps and p-Ps lifetimes. The knowledge of these quantities is of great interest for the physics of heavy quarkonia such as J/Ψ and Υ. Moreover, this requires considerably better experimental accuracy.

3. The *positronium spectrum* calculated taking into account high-order radiative corrections is also a good testing ground for QED.

As for anti-hydrogen, the item of main intereset in the positronium spectrum is measurement of the $1S-2S$ transition. The lifetime of positronium in the metastable $2S$ is eight times larger (the ratio of the squares of the wave functions at the origin for the first and second levels), than in the ground state, which permits a much higher accuracy.

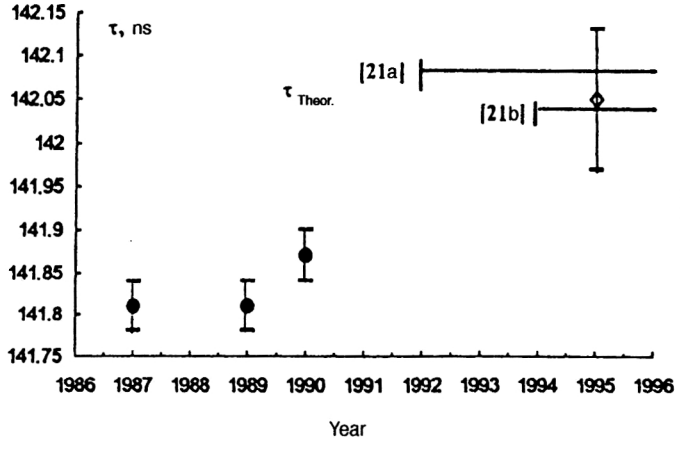

FIG. 1. Theoretical and experimental values of the orthopositronium lifetime. 1987–1990: studies by the Michigan group (Refs. 22–24); 1995: studies by the Tokyo group (Ref. 25).

Here mention should be made of the experiments[29,30] to measure the energy of the $1S-2S$ transition using Doppler-free two-photon spectroscopy. The accuracy attained $\Delta\varepsilon/\varepsilon\sim 1\times 10^{-8}$ is at the same level as that of the masses and electric charges of the electron and positron, but still inferior to that of the electron and positron gyromagnetic ratios, the electron magnetic moment (Table I), and also the hydrogen spectrum.

Precise measurement of the *fine structure* of the spectrum is very interesting. In particular, the difference between the energies of the ortho- and para-levels in the ground state (see Ref. 31 and references therein) is given by

$$\Delta\varepsilon_{FS}=2\pi\hbar\cdot\Delta\nu_{FS},$$

where

$$\Delta\nu_{FS}=\frac{\alpha^4mc^2}{2}\left[\frac{7}{6}-\frac{\alpha}{\pi}\left(\frac{16}{9}+\ln 2\right)+\frac{5}{12}\alpha^2\ln\left(\frac{1}{\alpha}\right)+a\frac{7\alpha^2}{6}-b\frac{\alpha^3}{\pi}(2\ln\alpha)^2\right]. \quad (1.6)$$

The coefficients $a\approx 0.0108$ and $b\approx 0.0021$ have not yet been fully calculated. The theoretical and experimental values coincide within one standard deviation taking into account the uncertainty in the theoretical value (Table II). The accuracy with which they are measured is 3.6 ppm.

The Michigan group[32] has performed precision measurements of the fine structure of the $2S-2P$ states of orthopositronium, and the results coincide with the theoretical values of the level splitting calculated through order α^3.

4. Fundamentally new results can be expected from experiments to seek orthopositronium annihilation with violation of momentum conservation and charge invariance:

$$o\text{-}Ps\rightarrow 2n\gamma, \quad (1.7)$$

where n is an integer. The current value of the upper limit on the decay probability (1.7) for $n=1$ (Ref. 33) can be significantly improved in experiments using positronium fluxes.

5. Just as interesting is the search for exotic and rare decay channels of parapositronium:

$$p\text{-}Ps\rightarrow n\gamma, \quad n>2. \quad (1.8)$$

The limit of the possibilities offered by standard experiments is apparently the case $n\geqslant 4$. The upper limit on the ratio of annihilation probabilities for $n=2$ and $n\geqslant 4$ obtained in Ref. 34 is consistent with the QED estimates.

6. The discrepancy between the theoretical and experimental values of the $o\text{-}Ps$ lifetime mentioned above has given rise to the hypothesized existence of a light, neutral, short-lived boson, via which $o\text{-}Ps$ annihilation can occur:

$$o-Ps\rightarrow b+\gamma$$
$$\quad\;\;\rightarrow 2\gamma. \quad (1.9)$$

The existence of such an $o\text{-}Ps$ decay channel should be manifested in the spectrum of detected γ quanta as a *narrow monochromatic peak* [see (6.14)], if the positronium is generated inside the target, as occurs in the usual experimental setup. It has been shown in experiments to seek this particle[35–38] that the decay probability (1.9) is less than $(1-2.8)\times 10^{-5}$ if $m_b<1$ MeV/c^2 (Fig. 2). The lifetime of the hypothetical boson with mass no greater than 30 KeV/c^2 is no more than $10^{-13}(m_bc^2)_{\text{keV}}$ sec.

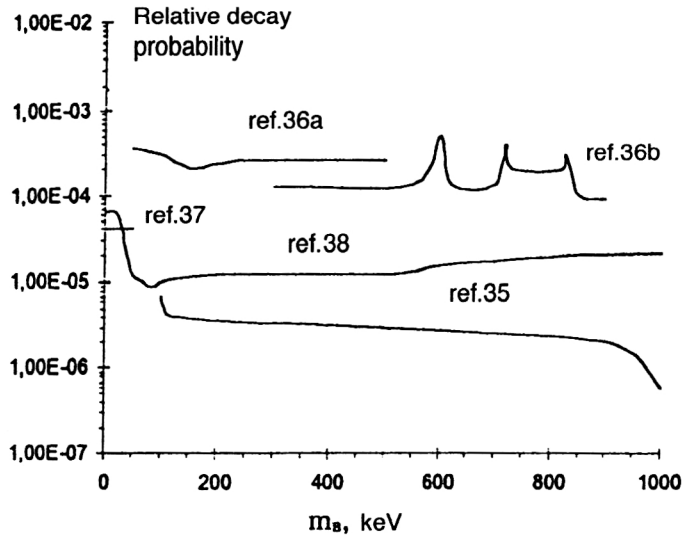

FIG. 2. Relative probability for orthopositronium annihilation with production of a short-lived neutral boson of mass m_b (results of Refs. 33–36).

7. Perhaps the most intriguing problem in positronium physics is the search for the *"mirror world"* hypothesized by the authors of Ref. 39. It was later suggested[40] that orthopositronium be used as the test object, because it is a particle with quantum numbers equal to zero. In particular, the mixing of $o\text{-}Ps$ and its analog from the mirror world would lead to the possibility of $o\text{-}Ps$ transitions from our world to the mirror world, so that $o\text{-}Ps$ would vanish without a trace from our observation. This would be seen as undercounting of the number of triple coincidences from anihilation γ quanta (see Sec. 6.5 below).

Amusingly, the $o\text{-}Ps$ escapees can be used to communicate with the mirror world (which would seem to be excluded by the hypothesis of Ref. 39). This would require time modulation of the $o\text{-}Ps$ beam.

The experimental limit on the probability for $o\text{-}Ps$ "disappearance" is currently estimated[41] to be no more than 10^{-3} of the probability for 3γ annihilation.

2. ANTIHYDROGEN PRODUCTION

2.1. The first experiment producing antihydrogen

In the experiment[3] performed at the LEAR antiproton storage ring at CERN, a circulating antiproton beam of energy 1.2 GeV (momentum 1.94 GeV/c) interacted with the xenon atoms of an internal cluster (jet) target. The target thickness reached 3×10^{13} atoms/cm^2, and the intensity of the antiproton beam was 1.7×10^{10} particles for a lifetime of 3 min. The integrated luminosity for September and October of 1995 was $5\times 10^{33}(\pm 50\%)$ cm^{-2}.

Atoms of antihydrogen ($\bar{H}^0$) appeared inside the target when antiprotons interacted with xenon nuclei: an antiproton interacting with a nucleus generates an e^+e^- pair (Fig. 3) and captures a positron if the momentum of the latter is close

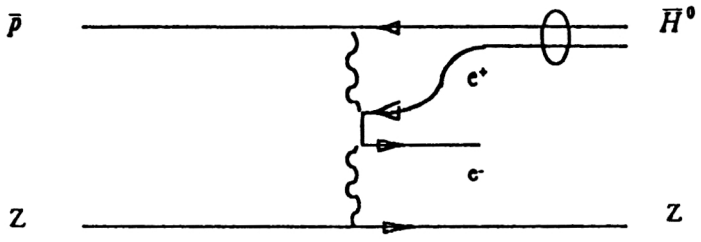

FIG. 3. Graph of two-photon e^+e^- production pair in the interaction of an antiproton with a nucleus and production of an antihydrogen atom.[3]

in magnitude and direction to that of the antiproton (an energy difference of less than 13.6 eV). The cross section for this process is

$$\sigma \sim 2Z^2\, pb \sim 6\cdot 10^{-33}\ \text{cm}^2, \qquad (2.1)$$

where $Z=54$ is the atomic number of xenon. Therefore, for the given luminosity, it could be expected that 30 atoms of $\bar{H}^0$ would be obtained. The fast, neutral $\bar{H}^0$ atoms (antiproton energy equal to 1.217 GeV and positron energy equal to 0.663 MeV), which were not deflected in the magnetic field of the storage ring, traveled into the detection channel (Fig. 4). Passing through the first two of three silicon counters Si (of thickness 700 μm and 500 μm, respectively), the $\bar{H}^0$ atoms lost the positron, which was stopped in one of the counters, producing a γ pair. The third counter recorded dE/dx from the remaining antiproton. The annihilation γ pair was recorded by a cylindrical NaI calorimeter (with energy resolution 14%), which covered 91% of the entire solid angle, thereby ensuring a total efficiency of 82%.

The antiprotons appearing after the stripping of the $\bar{H}^0$ atom passed through three start scintillators Sc (each 4 mm thick) and a hodoscope H of 16 fibers ($2\times2\times32$ mm), and then a group of four stop scintillators Sc (Fig. 4). The three drift chambers D with corresponding readout delays recorded the passage of antiprotons deflected in the dipole magnetic field B. The needed calibrations were performed using cosmic rays.

The experiment recorded **11** $\bar{H}^0$ atoms for a background contribution of no more than 2 ± 1 with 95% probability.

The main result of the experiment, namely, the proof of the "existence theorem," i.e., of the possibility of synthesizing antihydrogen atoms under terrestrial conditions, is certainly of fundamental importance.

2.2. Antihydrogen production in storage rings

The idea of producing beams (fluxes) of antihydrogen atoms is closely related to the technique of electron cooling.[1] For antihydrogen generation, the antiproton source, for example, one like the antiproton installations at CERN or Fermilab, must be provided with two storage rings. The first is used to store low-energy antiprotons and has a traditional system with hard focusing. In principle, LEAR at CERN can serve as such a storage device, although, of course, it has not been optimized for this purpose. The second is a positron storage ring of the racetrack type with four straight sections The storage rings are combined such that in one of the straight sections the beams pass through each other (Fig. 5), similar to what occurs in electron cooling devices.[1,2,5,6] This is where the antiprotons recombine, forming $\bar{H}^0$ atoms. Each storage ring has its own electron cooling system, allowing dense, cold beams of recombining particles to be obtained. *Positron production* also occurs on the electron cooling section. Its long-lived component, orthopositronium, can be extracted from the focusing system into the recording channel, similar to the $\bar{H}^0$ atoms (Fig. 5).

The proposed variant of positron storage ring[6,7] has a special focusing system with longitudinal quasiuniform and helical quadrupole magnetic fields. A bounding magnetic field consistent with the positron energy is also applied to the toroidal segments of this storage device. Such a focusing system of the "stellarator" type ensures stability of the beam of circulating electrons.

The fundamental feature of this scheme distinguishing it from those proposed earlier for low antiproton energies[2,42] is the magnetization of the positrons, whose source is also immersed in the longitudinal field. This complicates the injec-

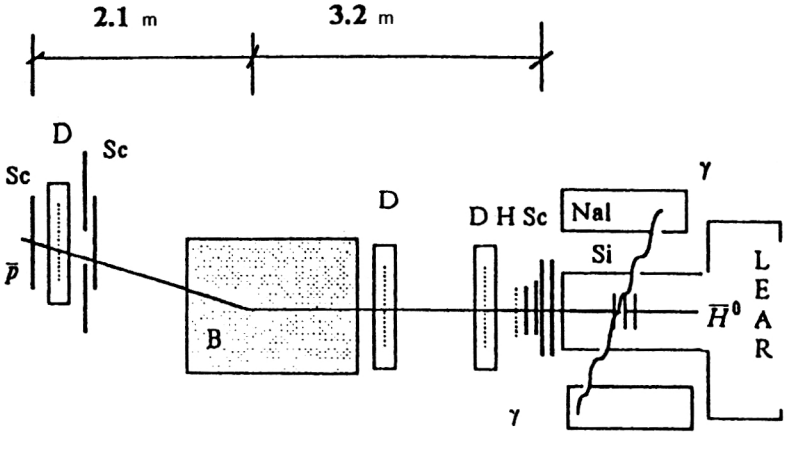

FIG. 4. Scheme for antihydrogen generation: Si—three silicon counters; Sc—silicon counter-trigger and scintillators; D—proportional chambers; NaI—6-section calorimeter; H—scintillation hodoscope; B—dipole magnet.

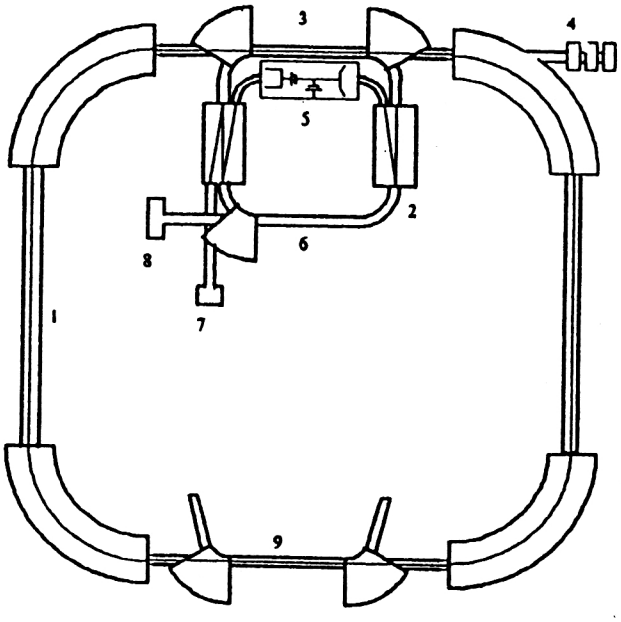

FIG. 5. Scheme for generating antihydrogen and positronium: *1*—antiproton storage ring; *2*—positron storage ring; *3*—$\bar{p}e^+$-recombination section; *4*—$\bar{H}^0$ detection channel; *5*—source and receiver of the electron beam; *6*—segment of electron cooling of positrons; *7*—positron injection channel; *8*—positronium detection channel; *9*—system for electron cooling of antiprotons.

tion of positrons into the ring, making it necessary to use a special injection system (see the description in Ref. 7). However, the magnetization leads to several important advantages.

First, the size of the positron beam is practically independent of the angular spread θ. This is related to the rather small value of the transverse Larmor radius of the positrons in the magnetic field B of the storage device:

$$\rho_\perp = \theta \cdot \frac{pc}{eB} \ll a, \tag{2.2}$$

where p is the positron momentum and $2a$ is the beam diameter.

The second advantage is the significant gain in the rate of electron cooling. The helical motion of the two particles in the magnetic field increases severalfold the number of collisions they undergo in traveling through the cooling segment.[43]

Finally, the design with magnetized beam is only weakly sensitive to retuning of the particle energy, which suggests that it might also be applicable for stabilizing the positron beam down to very low positron energies of the order of hundreds of eV (accordingly, antiproton energies of hundreds of keV). From the viewpoint of the stability of an intense beam, such a storage device is equivalent to a ring with very hard focusing, because the role of the betatron function in it is played by the Larmor helix, the period of which is of the order of several centimeters for the highest energy planned.

The electron cooling of the two beams of recombining particles, antiprotons and positrons, ensures low temperatures of each (small spread and velocity), thereby leading to a high recombination rate.[6,7]

Analysis shows that the intensity of the $\bar{H}^0$ flux is limited mainly by the deficiency of low-energy positrons. Three methods of positron production using a special target[44] are under consideration:[7]

1. A linear electron accelerator at an energy of about 40 MeV (the optimal value);

2. A source of hard synchrotron radiation with photon energy near the e^+e^--pair production threshold;

3. An intense positron-emitting radioactive source (such as ^{22}Na, ^{58}Co, and so on).

The second method offers the highest intensity, but it requires a storage device for electrons of energy of the order of GeV.

It should be stressed that the use of electron cooling makes it possible to obtain a *flux of* $\bar{H}^0$ *atoms with small angular spread in velocities*:

$$\frac{\Delta v_\perp}{v} \approx \frac{\Delta v_\parallel}{v} \approx \sqrt{\frac{T_\parallel}{2\varepsilon_p}}, \quad T_\parallel \approx e^2 n_e^{1/3} + \frac{T_C^2}{\beta^2\gamma^2 mc^2}, \tag{2.3}$$

where v and $\Delta v_{\perp,\parallel}$ are the average velocity of the $\bar{H}^0$ atoms and the spreads of its components, $T_\parallel$ is the electron "longitudinal" temperature and density in the particle rest frame, and ε_p is the antiproton kinetic energy, and T_C is the temperature of the electron given cathode.[6]

For positrons, in contrast to antiprotons, the temperatures associated with the longitudinal and transverse degrees of freedom are different owing to the positron magnetization. As a result of cooling, these temperatures become equal to those of the cooling electrons:[43]

$$T_\perp^+ \to (T_e)_\perp, \quad T_\parallel^+ \to (T_e)_\parallel. \tag{2.4}$$

Here $(T_e)_\perp \sim 0.1$ eV is the temperature of the electron transverse degree of freedom, roughly equal to the cathode temperature. For this reason, the cooled positron beam and, accordingly, the orthopositronium beam have relatively large angular spreads and small spreads in the longitudinal velocities (Table III).

Table III lists the design values of the parameters of storage rings and estimates of the intensities of antihydrogen and orthopositronium fluxes made in the radiative recombination approximation.[1)]

Yet another important advantage of systems with electron cooling, which follows from the equality of the average velocities of the cooling and cooled particles, is the possibility of *absolute calibration* of the $\bar{H}^0$-atom velocity (using the voltage at the cathode of the electron gun) and the possiblity of smooth, controlled *tuning* of this velocity within a broad range (using the same voltage or the potential of a "suspended" cooling segment). These possibilities are extremely important for performing the experiments discussed below.

3. DIRECT COMPARISON OF PARTICLE ELECTRICAL CHARGES

By measuring the displacement of the beam of atomic particles—antihydrogen, hydrogen, and positronium—emitted from the storage device and deflected in the trans-

TABLE III. Antiproton and positron storage ring parameters.

Antiproton storage ring		
Perimeter, m	80	
Antiproton energy, MeV	50	0.5
Density of cooling electron beam, A/cm^2	1.0	0.02
Electron longitudinal temperature, μ eV	120	70
Number of stored antiprotons	$1\cdot10^{11}$	$1\cdot10^{9}$
Antiproton current, mA	20	2.0
Positron storage ring		
Perimeter, m	20	
Positron energy, keV	27.2	0.272
Longitudinal magnetic field, T	0.1	0.05
Number of stored positrons	$1\cdot10^{9}$	$1\cdot10^{8}$
Positron beam current, μA	800	80
Density of cooling electron beam, A/cm^2	1.0	0.002
Intensity,sec^{-1}	$3\cdot10^{4}$	30
Angular spread, μrad	1.1	8.5
Velocity spread, 10^{-6}	1.1	8.5
Doppler spread,$\Delta v/c$, 10^{-7}	3.5	2.7
Orthopositronium flux		
Intensity, sec^{-1}	$1.7\cdot10^{4}$	35
Angular spread, mrad	1.5	16
Velocity spread, 10^{-5}	5.1	40
Doppler spread, 10^{-5}	1.5	1.2

verse magnetic field, it is possible to obtain an upper limit on the difference of the electric charges δe.[13] The sensitivity of the method is mainly determined by the accuracy of measuring the atomic coordinates δx at the channel exit:

$$\frac{\delta e}{e}=\frac{2pc}{eB_\perp}\cdot\frac{\delta x}{L^2}. \tag{3.1}$$

Here L is the length of the atom path in the transverse magnetic field $B_\perp$ and p is the atom momentum. The use of the "zero" measurement method—with the field and without the field—can provide a resolution of at least 0.1 of the total beam width in the detector:

$$\delta x\leqslant 0.1\theta_p L, \tag{3.2}$$

where θ_p is the angular spread of the atomic beam. Substituting $\theta_p=\Delta\nu_\perp/\nu$ from (2.3) into this, we see that the sensitivity (3.1) does not depend directly on the energy in the case of electron cooling of the antihydrogen (or hydrogen) atoms:

$$\left(\frac{\delta e}{e}\right)_{\bar{\mathrm{H}}^0}\leqslant 0.2\cdot\frac{\sqrt{Mc^2T_\parallel}}{eB_\perp L}, \tag{3.3}$$

where M is the antiproton mass.

Of course, the temperature of the cooling electrons $T_\parallel$ is different for different electron energies and currents. Nevertheless, there are some possibilities for maneuvering here: after cooling the antiproton beam by a sufficiently intense electron beam, it is possible to decrease its current and "squeeze out" a very small angular spread. If we take the values given in Table III for the angular spread, then in a field $B_\perp=10$ T the sensitivity becomes

$$(\delta e/e)_{\bar{\mathrm{H}}^0}\sim 2\cdot10^{-9}. \tag{3.4}$$

Here a resolution δx (3.2) of order 1–2 μm is required.

For positronium the value of $B_\perp$ is limited owing to interference between its ortho- and para-states accompanied by rapid annihilation of the p-Ps component (Sec. 6.1). Nevertheless, even in fields of order 1 T we can count on

$$(\delta e/e)_{Ps}\sim 1\cdot10^{-8}. \tag{3.5}$$

Of course, this value decreases the present limit only insignificantly (Table I). Nevertheless, by performing an experiment of this design with antihydrogen and positronium and using the high accuracy with which the charges e_p and e^- coincide, it is possible to "close" (via positronium!) the chain of charges of all four particles with an accuracy of at least 10^{-8}, i.e., to improve the inequality of e_p and e_a by three orders of magnitude (Table I). Further improvement is determined by the limit on the inequality of e^+ and e^-.

We should stress the fact that the proposed experiment gives the *difference of the electric charges* of the particles, and so it differs from the experiment of Ref. 15, where e/m is measured. The results of the two experiments allow the upper limit on the inequality of m_p and m_a to be improved.

4. SPECTROSCOPY OF THE $2S-2P$ STATES OF ANTIHYDROGEN

The methods of radiospectroscopy and atomic interferometry developed in measurements of the hyperfine structure and the Lamb shift of the hydrogen spectrum[8–12] can be used in these experiments.[13] These methods are part of the general approach based on the interference of two nearby states of an atom in an external electromagnetic field.

4.1. Interference in a two-level system

The behavior of a two-level quantum system under the influence of an external periodic perturbation with amplitude E and frequency ω close to the transition frequency ω_0 is quite well known (see Ref. 18). In the perturbing field the upper level u and lower level d form a single bound state, and the probabilities of finding the system in the states u and d after the perturbation is switched off depend on its parameters: the frequency, amplitude, and duration of the perturbation. The wave function of a two-level system in the field of an external perturbation can be found following Ref. 18 (see the problem in Sec. 40, where unfortunately there is an error in the solution) and introducing the decay constants of the states γ_u and γ_d. If at the initial time $t=0$ the system is in the lower state, i.e., $\Psi(0)=\Psi_d^0$, its state at time t is described by the wave function

$$\Psi_I(t)=\left[\frac{1}{2\Omega}\left(\Omega_d e^{(i\Omega_u-\alpha)t/2}+\Omega_u e^{-(i\Omega_d-\alpha)t/2}\right)\Psi_d^0 + \frac{\Omega_E}{\Omega}\left(e^{(i\Omega_d-\alpha)t/2}-e^{-(i\Omega_u-\alpha)t/2}\right)\Psi_u^0\right]e^{-(\gamma_u+\gamma_d)t}, \tag{4.1}$$

where $\Omega_{u,d}=\Omega\pm\Delta\omega$, $\Delta\omega=\omega-\omega_0$, $\Omega=\sqrt{(\Delta\omega)^2+4\Omega_E^2}$,

$$\alpha=\frac{\Delta\omega}{\Omega}(\gamma_u-\gamma_d),\quad \Omega_E=\frac{Ed_{ud}}{\hbar},\tag{4.2}$$

$\Psi^0_{u,d}$ are the wave functions of the unperturbed states, and $d_{u,d}$ is the matrix element of the $d-u$ transition, which for the hydrogen atom is equal in order of magnitude to the product of the electron charge and the Bohr radius a_0. For example, for the $2S-2P$ transition discussed below we have (see, for example, problem 11.56 of Ref. 46)

$$d_{2S-2P}=3ea_0.\tag{4.3}$$

Equation (4.1) is valid for

$$\Omega\gg\gamma_u,\gamma_d.\tag{4.4}$$

If at $t=0$ the system is in the u state $[\Psi(0)=\Psi^0_u]$, its perturbed wave function is described by Eq. (4.1) after interchanging the indices u and d:

$$\Psi_{II}(t)=\Psi_I(t)|_{u\leftrightarrow d}.\tag{4.5}$$

The probability of finding the system $\Psi_I(t)$ in one of the two (u or d) states is equal to the squared modulus of the expression in front of the corresponding unperturbed function in (4.1):

$$P^{(I)}_d(t)=\frac{1}{4\Omega^2}(\Omega_d^2e^{-\alpha t}+\Omega_u^2e^{\alpha t}+8\Omega_E^2\cos\Omega t)\cdot e^{-(\gamma_d+\gamma_u)t},$$

$$P^{(I)}_u(t)=\frac{2\Omega_E^2}{\Omega^2}(\cosh\alpha t-\cos\Omega t)e^{-(\gamma_d+\gamma_u)t}.\tag{4.6}$$

We stress the fact that γ_u and γ_d are the decay constants of the states entering into the expressions for the wave functions. They are half the corresponding *level widths*, or the inverse lifetimes of the states:

$$\gamma_{u,d}=\Gamma_{u,d}/2.\tag{4.7}$$

Equation (4.6) clearly demonstrates the effect of producing a bound state, when the system makes a transition from the d state to the u state and vice versa. This is completely obvious in the case of small level widths $\gamma_{u,d}\to 0$:

$$P^{(I)}_d=\frac{\Delta\omega^2}{\Omega^2}+\frac{2\Omega_E^2}{\Omega^2}(1+\cos\Omega t),$$

$$P^{(I)}_u=2\frac{\Omega_E^2}{\Omega^2}(1-\cos\Omega t)=1-P^{(I)}_d.\tag{4.8}$$

This interference of states is a quite general quantum-mechanical phenomenon and is observed in all the fundamental interactions (see, for example, Ref. 47).

Later on, in discussing the physics of positronium (Sec. 6.1), we shall need the expressions for the probabilities (4.6) in case II, when initially the system is in the u state. Let us write these expressions in a form different from (4.6):

$$P^{(II)}_u(t)=\frac{1}{4\Omega^2}(\Omega_u^2e^{-\Gamma'_ut}+\Omega_d^2e^{-\Gamma'_dt}+8\Omega_E^2\cos\Omega t\cdot e^{-\Gamma t}),$$

$$P^{(II)}_d(t)=\frac{\Omega_E^2}{\Omega^2}(e^{-\Gamma'_ut}+e^{-\Gamma'_dt}-2\cos\Omega t\cdot e^{-\Gamma t}),\tag{4.9}$$

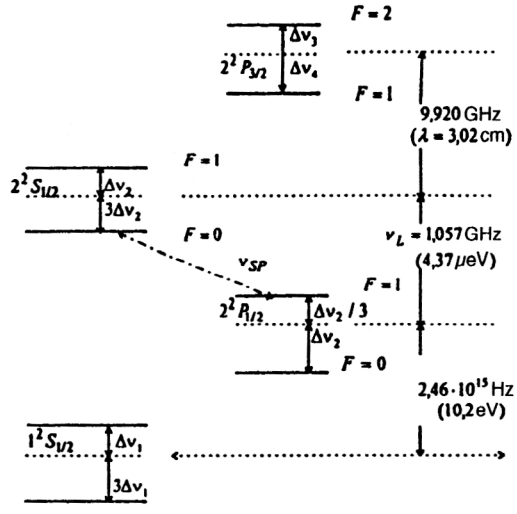

FIG. 6. Structure of the low-lying levels of the hydrogen atom. $\Delta\nu_1=355.1014$ MHz, $\Delta\nu_2=\Delta\nu_1/8$, $\Delta\nu_3=\Delta\nu_2/10$, $\Delta\nu_4=(13/30)\Delta\nu_2$, $\nu_L=1057.8514(19)$ MHz is the Lamb shift.

where we have introduced the decay constants

$$\Gamma'_u=\frac{\Omega_u\Gamma_u+\Omega_d\Gamma_d}{2\Omega},\quad \Gamma'_d=\frac{\Omega_u\Gamma_d+\Omega_d\Gamma_u}{2\Omega},$$

$$\Gamma=\frac{\Gamma_u+\Gamma_d}{2}.\tag{4.10}$$

For case II $[\Psi(0)=\Psi^0_u]$, Eqs. (4.8)–(4.10) are valid after interchange of the indices u and d.

Equations (4.9) show that a mixed state decays with a constant which is a linear combination of the decay constants of the unperturbed states. This becomes especially important when one of the constants is much larger than the other: the lifetime of the long-lived state cancels out. In particular, this is important for positronium in a magnetic field (Sec. 6.1).

4.2. Radiospectroscopy of the $2S_{1/2}$ state. The atomic interferometer

The radiospectroscopic method developed in precision measurements of the hyperfine structure of the hydrogen atom[9] can also be used in experiments involving an antihydrogen flux. The idea of the method is that an external perturbation can be used to excite transitions between hyperfine levels of the metastable $2^2S_{1/2}$ state (whose lifetime is 1/7 sec), and then the resonance frequency of the transition can be measured. The atoms which have undergone this transition are detected by exciting the next transition from the $2S$ state to one of the short-lived 2^2P states (whose lifetime is about 1.5 nsec) with the decay of this state detected using the $2P\to 1S$ transition (Fig. 6). We shall call the device effecting this $2S-2P$ transition an "analyzer" (see the discussion at the end of this section). The frequencies of $2S-2P$ transitions lie in the centimeter wavelength region, and those of $2P\to 1S$ transitions lie in the vacuum ultraviolet (10.2 eV).

The main difference between the experiment discussed here and the pioneering one of Ref. 9 is the relatively high

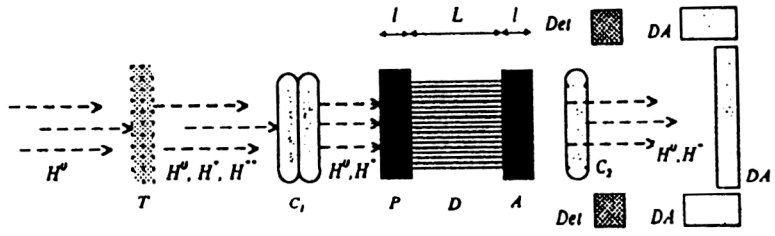

FIG. 7. Scheme for an atomic interferometer: $\bar{H}^0$, H*, $\bar{H}$* are antihydrogen atoms in the ground and excited states; T is a thin target; P and A are cavities for purification and analysis. The interferometer: l is the length of cavities C_1 and C_2; L is the length of free space (D); Det are UV-radiation detectors; DA are annihilation detectors.

velocity of the atoms, v_0. This affects the resolution of the method, and also makes it necessary to take into account the Doppler frequency shift:

$$\omega_{\text{Lab}}=\frac{\omega'}{\gamma(1-\beta\cos\theta)},\quad \gamma=(1-\beta^2)^{-1/2},\quad \beta=v_0/c. \tag{4.11}$$

Here ω' is the frequency in the atomic rest frame and θ is the angle between the directions of the atomic velocity and the cavity axis.

For the numerical estimates below we shall use the two extreme cases given in Table II:

$$\text{"fast atoms"}:\varepsilon=50\ \text{MeV},\quad \beta=0.31,\quad \gamma=1.0533,$$

$$\text{"slow atoms"}:\varepsilon=0.5\ \text{MeV},\quad \beta=0.03,\quad \gamma=1.0005. \tag{4.12}$$

Let us assume that we have, by some method (see below), succeeded in forming a beam of atoms in the lower $2^2S_{1/2}(F=0)$ state, which is passed through a cavity tuned to the frequency corresponding to that of the transition in the atomic rest frame.

At the cavity output the flux of atoms in the upper $2^2S_{1/2}(F=1)$ state is

$$\dot{N}_{2P}=\dot{N}_{Al}\cdot P_u^{(1)}(\tau), \tag{4.13}$$

where $\dot{N}_{Al}$ is the flux of atoms at the cavity input, $P_u^{(1)}(\tau)$ is the probability (4.8), and $l=v_0\tau$ is the cavity length. After passing through the resonator, the atoms reach the analyzer, where they make a transition into the $2P$ state and decay over a short distance v_0/Γ_{2P} (15 cm for fast atoms and 1.5 cm for slow ones). Therefore, the counting rate simply coincides with the atomic flux (4.13), taking into account the correction for the detector efficiency. Eliminating the dependence of the counting rate on the cavity frequency, we can determine the resonance frequency corresponding to the transition frequency. The maximum counting rate is attained if the field amplitude satisfies the equation

$$\Omega_E\tau=\frac{\pi}{2}. \tag{4.14}$$

Here the frequency dependence of the counting rate is described by a smooth function [see Eq. (4.8)]:

$$\dot{N}_{2P}=\dot{N}_{Al}\left(\frac{\sin(\sqrt{1+x^2}\pi/2)}{\sqrt{1+x^2}}\right)^2,\quad x=\frac{\Delta\omega}{2\Omega_E}. \tag{4.15}$$

The half-width of this function is of order

$$\Delta\omega_{1/2}\approx\pm\frac{\pi}{\tau}. \tag{4.16}$$

The accuracy (resolution) can be improved by many orders of magnitude by using the technique of the *atomic interferometer*.[8–10,12]

The operating principle of such an interferometer, which was apparently first proposed in Ref. 8, is the following. Two short electromagnetic field pulses, separated in space and time by a relatively long interval $L=v_0T$, are applied; between them, the atom moves in free space. In the radiospectroscopic version of this interferometer these pulses are generated by the electromagnetic fields of two cavities (Fig. 7) excited at the same frequency ω. The first cavity C_1 induces, as before, transitions between initial "lower" $2^2S_{1/2}(F=0)$ states and final "upper" $2^2S_{1/2}(F=1)$ states. The phase of the wave function at the output of C_1 depends on the resonator length l, the frequency, and the field amplitude. After passing through the free segment L, the atom enters the second cavity C_2, where it again undergoes transitions between the two states. The atoms leaving the interferometer in the "upper" state undergo transitions to the $2P$ state in the analyzer and deexcite to the $1S$ state. The photons of the UV radiation are recorded by the detectors Det.

The probability of finding an atom in the upper state at the interferometer output can be obtained by matching the corresponding wave functions at the junctions of the three interferometer segments. In the simplest case of small level widths ($2S$ state!)

$$\Gamma\tau\leqslant\Gamma T\ll 1,\quad P=P_{u,d}, \tag{4.17}$$

we find

$$P_u(\omega)=\left(\frac{4\Omega_E}{\Omega}\sin\frac{\Omega\tau}{2}\right)^2\cdot\left(\cos\frac{\Omega\tau}{2}\cdot\cos\frac{\Delta\omega T}{2}-\frac{\Delta\omega}{\Omega}\sin\frac{\Omega\tau}{2}\cdot\sin\frac{\Delta\omega T}{2}\right)^2\xrightarrow{\Delta\omega\to 0}\sin^2 2\Omega_E\tau. \tag{4.18}$$

The quantities Ω, Ω_E, and $\Delta\omega$ have the same values as in (4.2).

The half-width of the function (4.18) with the condition (4.17) is

$$\Delta\omega_{1/2}\approx\frac{1}{T}. \tag{4.19}$$

At first sight the gain relative to (4.16) appears insignificant. However, the length of the free segment L can be chosen to be much longer than the cavity length l (i.e., $T\gg\tau$). In addition, the accuracy of determining the transition frequency ω_0 can be raised considerably if the dependence $P_u(\omega)$ is measured (Fig. 8). By fitting the experimental data to the

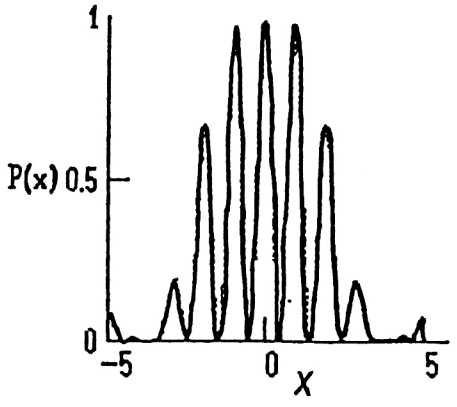

FIG. 8. Signal from the atomic interferometer [Eq. (4.14)], $T/\tau=3$, $x=\Delta\omega\tau/2$.

function (4.18), it is possible to raise the accuracy to nearly $\sqrt{N}$, where N is the total number of experimental points.

The best accuracy is achieved in this manner in Ref. 9. The authors of that study obtained a resolution of order 50 Hz, which allows measurement of the hyperfine structure of the $2S_{1/2}$ state with an accuracy of order

$$\frac{\delta\omega}{\omega}\sim 3\cdot 10^{-7}. \tag{4.20}$$

Zeeman splitting and double fitting were used for this (see Sec. 4.4).

Let us make a few remarks about the experimental setup. Measurement of the described transition requires a flux of $\bar{H}^0$ atoms in the corresponding excited $2^2S_{1/2}(F=0)$ state. Such a flux can be formed using a thin target of foil[10,11] or a gas jet, which the atoms collide with to induce transitions to excited states. Then the flux is subjected to a special purification process: it is passed through a "polarizer" (Ref. 10, for example), resonators which induce transitions from the "useless" $2^2S_{1/2}(F=1)$ state to the $2P_{1/2}$ state (of frequencies 1147 and 1087 MHz) followed by transitions to the $1S$ level. After this process, the beam contains predominantly atoms in the $2^2S_{1/2}(F=0)$ state, and the hyperfine splitting of this level is then measured by an interferometer and the cavity C_2, using transitions to the $2^2P_{1/2}$ or $2^2P_{3/2}$ level.

The authors of Ref. 9 used an original technique for purifying ("polarizing") the flux and analyzing it by means of a magnetic field. For a certain value of the field strength, the Zeeman splitting causes the energies of the $2^2S_{1/2}(F=0)$ and $2^2P_{1/2}(F=1)$ states to coincide, which induces transitions to the $1S$ state. The transition from the u state to the d state of the $2S$ level was studied for this case.

The photons of the UV radiation arising in deexcitation of the atoms from the $2P$ state are recorded in coincidence (taking into account the time of flight) with the signals of the counters recording the radiation arising in the annihilation of the particles of the $\bar{H}^0$ atom—the antiproton and the positron—when they reach the detector wall DA. This procedure is similar to the one used in the first experiment on antihydrogen synthesis (Sec. 2.1).

Determination of the values of the hyperfine splitting of the $2S_{1/2}$ level of hydrogen and antihydrogen allows [see (1.2)] comparison of the proton and antiproton magnetic moments at a level $10^{-6}-3\times10^{-7}$.

4.3. The Lamb shift of the 2P level. The atomic interferometer with electrostatic

A variant of the atomic interferometer with static electric fields was successfully used in experiments[10] involving hydrogen atoms of low energy of order 20 keV. The goal of the study was measurement of the Lamb shift of the $2P$ state (Fig. 6). The frequency of the transition $2^2S_{1/2}(F=0)\rightarrow 2^2P_{1/2}(F=1)$ was measured (this is labeled as ν_{SP} in Fig. 6). Knowledge of the frequencies of all possible transitions between the $2S$ and $2P$ levels makes it possible to find the Lamb shift:

$$\omega_L=\omega_{SP}+3\Delta\omega_2+\frac{\Delta\omega_2}{3}. \tag{4.21}$$

The values of the frequency $\Delta\omega_2$ were taken from Ref. 9.

This interferometer variant differs from the one described above in that the ac electromagnetic field of the cavities is replaced by the dc field of two capacitors or dc two pairs of diaphragms. The states in question mix in these fields owing to the Stark effect. The interlevel transitions are described by Eqs. (4.1)–(4.18) with the substitution

$$\omega=0,\quad \Delta\omega=\omega_0,\quad \Omega=\sqrt{\omega_0^2+4\Omega_E^2}. \tag{4.22}$$

Here, as before, ω_0 is the transition frequency, and the expression for Ω_E has the same form as in (4.2)–(4.3), with the only difference that now E is the strength of the static field. By measuring, as in Sec. 4.2, the dependence of the flux of atoms in the $2^2P_{1/2}$ state on the field strength E or the time of flight T (for which it is necessary to vary the atomic velocity, by varying, for example, the energy of the cooling electrons), it is possible to find ω_0 by a fit to the function (4.18). The accuracy of measuring the transition frequency attained in Ref. 10 was $\delta\omega_{SP}=2\pi\cdot 2$ kHz.

A feature of this spectrometer variant is the fact that $\Delta\omega=\omega_0=\text{const}$ [see (4.18)], so that to obtain the maximum counting rate, in addition to the condition (4.14), it is necessary to choose the electric field strength such that

$$\Omega_E\approx\omega_0. \tag{4.23}$$

For $2S-2P$ transitions this gives

$$E\approx\frac{\hbar\omega_L}{3ea}=291\ \text{V/cm}. \tag{4.24}$$

We note that the Doppler spread of frequencies in the experiment of Ref. 10 was about 3×10^{-5} of the transition frequency.

The first measurements of the Lamb shift with a flux of fast ($\nu_0/c\approx0.35$) hydrogen atoms were performed at a proton storage ring with electron cooling, NAP-M.[11] The low accuracy of the experiment was mainly due to insufficient statistics.

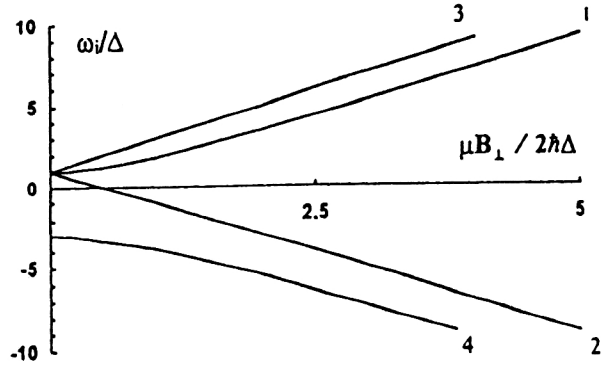

FIG. 9. Hyperfine structure of the ground state of hydrogen in a magnetic field: $m=1$ (*1*), -1 (*2*), 0 (*3* and *4*).

4.4. The atomic interferometer and the Stern–Gerlach method. Spectroscopy of the 1*S* state

The use of the atomic interferometer in the classical Stern–Gerlach method made it possible to perform high-precision measurements of the hyperfine structure of the ground $1^2S_{1/2}$ state of the hydrogen atom.[12] This scheme can be applied nearly without change in experiments involving antihydrogen fluxes. For this the polarizer and analyzer of the interferometer (Fig. 7) must be realized as ordinary EPR spectrometers: each must consist of a dipole magnet with a uniform field $B_\perp$ directed across the beam, and a resonator in which an electromagnetic field is produced. Its magnetic component $B_g(t)=B_g \sin \omega t$ excites EPR transitions. In addition, a sorting system composed of two gradient magnets, one before and one after the analyzer, is provided. The magnets separate atoms with different polarization (the Stern–Gerlach method), and guide atoms in a given state to the detector. The transition from one state to another is accompanied by change of the polarization, as a result of which the atom is sent to the detector by the second sorting magnet. In the current version, the gradient sorting magnets are made in the form of sextupoles as, for example, in the hydrogen maser—the time standard.

The hyperfine structure of the $1S$ state of the hydrogen atom in a magnetic field is well known. The level is split into 4 sublevels, the energy (frequency) of which depends on the value of the field $B_\perp$ (Fig. 9):

$$\omega_{1,2}=\Delta\pm\frac{\mu B_\perp}{\hbar}, \quad m_F=\pm 1,$$

$$\omega_{3,4}=-\Delta\pm 2\sqrt{\Delta^2+\left(\frac{\mu B_\perp}{2\hbar}\right)^2}, \quad m_F=0,$$

$$\mu=\begin{cases}\mu_e-\mu_p, & \mu_F=\pm 1\\ \mu_e+\mu_p, & \mu_F=0,\end{cases} \tag{4.25}$$

where

$$4\Delta=\Delta\omega_{HFS}=2\pi\times 1.420\ 450\ 751\ 800(28)\ \text{GHz}$$

is the hyperfine splitting for $B_\perp=0$ and μ_e and μ_p are the electron and proton magnetic moments. For example, for $B_\perp=0.1$ T, the frequency of the $1\leftrightarrow 2$ transition accompanied by complete spin flip (of the electron and proton) is about 2.8 GHz.

As before, Eq. (4.18) describes the intensity of the flux in the u state for the substitution

$$\Omega_E\to\omega_g=\frac{\mu B_g}{\hbar},$$

$$\Delta\omega=\omega_0-\omega, \tag{4.26}$$

where $\omega_0=|\omega_i-\omega_k|$ is the frequency of the transition between levels 1–4 [Eq. (4.25) and Fig. 9].

A double fit of the experimental results—the dependence of the intensity of the flux passing through the interferometer to Eq. (4.18) and then the dependence $\omega_0(B_\perp)$ to Eq. (4.25)—greatly increases the accuracy. It can be hoped that this will allow the Doppler-broadening limit (see Table III) to be exceeded by an order of magnitude, giving

$$\delta\omega/\omega_0\leqslant 3\cdot 10^{-8}. \tag{4.27}$$

The use of Zeeman splitting in high-precision radiospectroscopic measurements is a fairly common technique which can also be applied successfully in the spectroscopy of excited states.[9,12] The techniques described in Secs. 4.2 and 4.4 essentially differ only in the method of detecting atomic transitions.

We note that the motion of a fast atom in a magnetic field $B_\perp$ generates an electric field in the frame of the atom:

$$E'_{\perp\perp}=\beta\gamma B_\perp,$$

which induces the Stark effect. This effect can be eliminated (up to the spread of atomic velocities $\Delta v/v$) by imposing a transverse electric field

$$E_{\perp\perp}=-\frac{1}{\gamma}E'_{\perp\perp}=\beta B_\perp. \tag{4.28}$$

However, this somewhat weakens the magnetic field in the frame of the atom:

$$(B'_\perp)_{\text{tot}}=\frac{B_\perp}{\gamma}. \tag{4.29}$$

Knowledge of the frequency of transitions between hyperfine levels of the ground state makes it possible to determine the value of the antiproton magnetic moment using (4.25):

$$\mu_a=\frac{1}{2}(\mu(m_F=0)-\mu(m_F=\pm 1)). \tag{4.30}$$

The accuracy of this determination is obviously

$$\frac{\Delta\mu_a}{\mu_a}\sim\frac{\Delta\mu}{\mu_a}\sim\frac{\mu_e}{\mu_a}\cdot\frac{\delta\omega}{\omega_0},$$

which for the accuracy (4.27) gives $\Delta\mu_a/\mu_a\sim 2\times 10^{-5}$.

Higher accuracy can be obtained by comparing the values of the hyperfine splitting Δ. Measurement of Δ for the antiproton with the accuracy (4.27) allows the difference between μ_p and μ_a [see (1.2)] to be found with an accuracy of at least 1×10^{-7}.

Let us conclude this section by mentioning the extremely high accuracy of the measurement of the hyperfine splitting of the ground state of *hydrogen* attained in experiments using atoms stored in magnetic traps: $\delta\omega/\omega_0 \sim 10^{-12}$. It is expected that the use of this technique for *antihydrogen* will involve serious difficulties, primarily in the capture and cooling of antiatoms in the trap. Nevertheless, here we can also hope for progress in the foreseeable future.

5. THE LASER SPECTROSCOPY OF FAST ANTIHYDROGEN ATOMS

The laser spectroscopy of antihydrogen atoms should be discussed seriously, in spite of the seeming hopelessness of the situation owing to the low intensity of the atomic fluxes. Estimates show that in the variants of the setup described below, the experiment is of great interest. This is primarily true of two-photon excitation of the $1S-2S$ transition, which is interesting because the metastable $2^2S_{1/2}$ level has extremely small width (a lifetime of 1/7 sec).

In working with a directed flux of fast atoms, by using a laser beam opposing the flux it is possible to raise the photon energy in the frame of the atom by way of the Doppler shift:

$$\omega' = \gamma(1+\beta)\omega, \quad \text{or} \quad \beta = \frac{(\omega'/\omega)^2-1}{(\omega'/\omega)^2+1}. \tag{5.1}$$

This means helps to compensate for the limitations in the choice of available lasers, and, as noted in Sec. 2.2, it also ensures *smooth tuning of the photon energy* in the frame of the atom, by changing the energy of the cooling electrons and, accordingly, the atomic velocity. This method is fairly simple and routine in the technique of electron cooling. It eliminates the necessity of using complicated, low-power dye lasers, which are commonly used in spectroscopy to vary the wavelength of the radiation.

5.1. The $1S-2S$ two-photon transition

The possibility of a $1S-2S$ two-photon transition in the scattering of an opposing laser beam on a flux of hydrogen atoms has been discussed some time ago in Ref. 2. The authors arrived at a pessimistic conclusion owing to the very low, of order several atoms/sec, intensity of the $\bar{H}^0$ flux in the antihydrogen generation scheme that they proposed. In the version discussed in the present study it actually becomes feasible to perform such an experiment.

The probability for a two-photon transition between levels m and n is[48]

$$W^{(2)}_{mn} = |Z^{(2)}_{mn}| \left(\frac{E}{\hbar}\right)^4 \cdot \frac{\Gamma_m/2}{(2\omega-\omega_{mn})^2+(\Gamma_m/2)^2}, \tag{5.2}$$

where

$$Z^{(2)}_{mn} = \frac{1}{2}\sum_l \frac{Z_{ml}Z_{ln}}{\omega_{ln}-\omega}$$

is the sum over all possible states between levels m and n to which transitions from the mth or nth level are allowed, Z_{ml} is the dipole matrix element of the transition $m \leftrightarrow l$, ω_{mn} is the frequency of the mn transition, Γ_m is the width of the mth level, and E is the amplitude of the electric field of the radiation. For the $1S-2S$ transition (with intermediate $2P_{1/2}$ level) we find

$$W^{(2)}_{1S2S} \approx 5 \cdot \left(\frac{eEa_0}{\hbar}\right)^4 \cdot \frac{1}{\omega_0^2} \cdot \frac{\Gamma}{\Delta\omega^2+(\Gamma/2)^2}. \tag{5.3}$$

Here a_0 is the Bohr radius, ω_0 is the frequency of the $1S-2S$ transition, $\Delta\omega = 2\pi\Delta f$ is the bandwidth of the radiation, and $\Gamma \approx 7\ \text{sec}^{-1}$ is the width of the $2S$ level. Assuming that $\Delta\omega \gg \Gamma$ and expressing E in terms of the density of radiated power, we find

$$W^{(2)}_{1S2S} \approx \frac{2}{(\Delta f)^2} \cdot \left(\frac{dP}{dS}\right)^2_{\text{W/cm}^{-2}}, \quad \text{sec}^{-1}. \tag{5.4}$$

Therefore, the transition probability is proportional to the square of the spatial–spectral density of the radiated power.

Equations (5.3) and (5.4) are written in the frame of the atom. In the laboratory frame the number of transitions per unit time in a flux $\dot{N}_{Al}$ propagating with speed βc counter to the ratiation is then

$$(\dot{N}^*) \approx 2\gamma \frac{(1+\beta)}{\beta} \cdot \left(\frac{d^2P}{dSdf}\right)^2_{\text{W}\cdot\text{cm}^{-2}\cdot\text{sec}} \cdot \frac{L}{c}\dot{N}_{Al}, \quad \text{sec}^{-1}. \tag{5.5}$$

Here L is the length of the bombardment segment. For $d^2P/dSdf \sim 100\ \text{W}\cdot\text{cm}^{-2}\cdot\text{sec}$, $\dot{N}_{Al} \sim 3\times 10^4$, $L = 5$ m, and $\beta = 0.64$ (see below for the choice of laser), Eq. (5.5) gives

$$\dot{N}^* \sim 30\ \text{sec}^{-1}.$$

The experiment can be set up as follows (Fig. 10). By means of a refracting cone, an axicon, laser light is directed counter to a beam of $\bar{H}^0$ atoms. The axicon has a hole at its center. Atoms excited by the radiation arrive at the cavities C tuned to the frequencies of $2S-2P$ transitions. After undergoing a transition to a short-lived $2P$ state, the atoms deexcite, and the rest of the procedure for detecting them is, in principle, analogous to that described in Sec. 2.1: the photons of $2P-1S$ transitions are recorded in coincidence (with time-of-flight selection) with signals from the detectors of the annihilation and ionization chambers. Therefore, the *integrated flux* of UV photons is recorded as a function of the velocity of the $\bar{H}^0$ atoms.

The background of scattered laser radiation can be lowered significantly owing to the same Doppler shift of the wavelength of the radiation from the moving atoms. The photon wavelength and flux depend on the direction of the emission in the laboratory frame (the angle θ, Fig. 10):

$$\lambda_{\text{lab}} = \gamma(1-\beta\cos\theta)\lambda_0, \tag{5.6}$$

$$\frac{d\dot{N}_\gamma}{d\Omega} = \frac{\dot{N}^*}{\gamma^2(1-\beta\cos\theta)^2}, \tag{5.7}$$

where $\lambda_0 = 2\pi c/\omega_0$ is the wavelength of the radiation in the frame of the atom. It follows from this and from (5.1) that in the laboratory frame the wavelength of the atomic radiation is shorter than that of the laser radiation; they are comparable

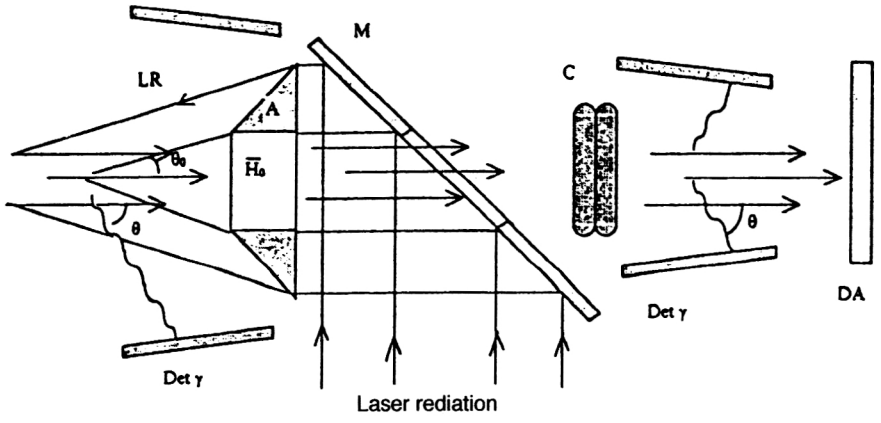

FIG. 10. Scheme for an experiment on the optical spectoscopy of antihydrogen atoms: $\bar{H}^0$ is the beam of antihydrogen atoms; LR is laser radiation; M is a mirror; A is a conical "prism," an axicon; C is a resonator exciting $2S-2P$ transitions; Det γ are UV-photon detectors; DA are detectors of the radiation arising in the annihilation of the $\bar{H}^0$ atom, an antiproton and a positron, on the detector walls.

only for photons scattered strictly backward. The atomic radiation is primarily directed forward. The photon flux in the forward hemisphere is

$$\Delta\dot{N}_\gamma=\frac{1+\beta}{2}\dot{N}^*. \tag{5.8}$$

A critical question is that of the choice of laser, because for the $1S-2S$ transition, even in two-photon excitation, a laser with wavelength near 240 nm is needed. The closest candidate is the KrCl excimer laser ($\lambda=222$ nm). Unfortunately, the power of excimer lasers is low, and their continuous single-mode operation is problematic. The Doppler shift (5.1) and colliding atomic–laser beams can be used, as shown in Fig. 10. In particular, to reach the region of the most powerful continuously operating laser, the argon laser (514 nm), atoms with antiproton energy of about 280 MeV are needed ($\beta=0.64$). It is quite possible to reach this energy in the proposed scheme of antihydrogen generation.

Finally, the resolution of the method remains the main question. The $1S-2S$ transition is interesting because the small width of the $2S$ level makes it possible, in principle, to measure the transition frequency with an accuracy

$$\frac{\delta\omega}{\omega}\leqslant\frac{\Gamma}{\omega}\sim 10^{-17}, \tag{5.9}$$

as pointed out by the authors of Ref. 4. The best accuracy attained for this transition in hydrogen (Ref. 49)[2)] is 1×10^{-11}. The authors of that study use a scheme with cancellation (in first order) of the Doppler frequency broadening, referred to as Doppler-free spectroscopy:[50] two laser beams are used, with one propagating along the atomic beam and the other opposite it. In the scheme of center propagating atom–laser beams discussed above, the Doppler broadening plays the decisive role.

It can be estimated by including in (5.1) the angular spread of the $\bar{H}^0$ beam $\Delta\theta$ and the longitudinal velocity spread of the atoms $\Delta\nu/\nu$:

$$\omega'=\gamma(1+\beta\cos\theta)\omega\approx\gamma(1+\beta\cos\theta_0)\omega \times\left(1+\beta\gamma^2\frac{\Delta\nu}{\nu}-\frac{\beta}{1+\beta}\left(\theta_0\cdot\Delta\theta+\frac{\Delta\theta^2}{2}\right)\right), \tag{5.10}$$

where $\theta_0\ll1$ is the beam intersection angle (Fig. 10). It follows that for a beam with the parameters given in Table III, the dominant factor is the spread in longitudinal velocities, which produces a Doppler frequency spread of order

$$\frac{\delta\omega'}{\omega'}\approx\beta\gamma^2\frac{\Delta\nu}{\nu}\approx10^{-7}. \tag{5.11}$$

The fitting technique described in Sec. 4 allows this limit to be exceeded by at least an order of magnitude, to reach an accuracy of 10^{-8}.

The Doppler-free scheme can be used in these experiments if it is somehow possible to solve the laser problem. Unfortunately, use of the Doppler shift as suggested above is not possible at present, because the Doppler-free scheme presupposes the excitation of a two-photon transition in an atom bombarded by two colliding beams of the same laser, one beam directed along the atomic flux, and the other opposite to it. Therefore, the Doppler shifts have different signs for each beam. This is actually the main idea of this scheme: the total energy (frequency) of two colliding photons in the frame of the atom [see Eq. (4.11)] is independent of the angular spread of the beam and, in a first approximation, of the velocity spread:

$$\omega_1'+\omega_2'=2\gamma\omega_{\text{laser}}.$$

Here ω_{laser} is the frequency of the laser radiation in the laboratory frame. The spread in the longitudinal velocities enters only through the factor γ, and, instead of Eq. (5.11), we have

$$\frac{\delta\omega'}{\omega'}\approx\gamma^2\beta^2\frac{\Delta\nu}{\nu}.$$

Although in a system for electron cooling of antiprotons an electron beam with adiabatically slow acceleration is used (see Refs. 6, Section 4.2), the contribution of fluctuations that determine the ordinary temperature of the electrons (the first term in the expression for $T_\parallel$ (formula (2.3) becomes negligible. In this case we have from Eq. (2.3)

$$\frac{\Delta\nu}{\nu}\sim\frac{T_C}{\sqrt{4\varepsilon_p\varepsilon_e}}\quad\text{and}\quad\frac{\delta\omega'}{\omega'}\sim\sqrt{\frac{m}{M}}\frac{T_C}{mc^2}\sim5\times10^{-9},$$

if $T_C\sim0.1$ eV (a beam from a thermionic cathode. The use of a special beams with photocathodes and fitting of the Doppler line broadening will yield a resolution at the 10^{-11}

level. An important point is that the resolution in this formulation of the experiment is nearly independent of the velocity of the antihydrogen atoms.

5.2. The $2S-4S$ two-photon transition

This transition, which was studied as an object of measurement in Ref. 4, lies in the visible region: its wavelength is 486 nm, so that the choice of laser does not present a serious problem.

For example, the argon laser used in the scheme discussed in Sec. 5.1 requires an antiproton energy of only 1.4 MeV.

The width of the $4S$ level is[51]

$$\Gamma_{4S}=4.3\times 10^{6}\ \text{sec}^{-1}.$$

Using the fact that the most probable two-photon $2S-4S$ transition is via the $3P$ level, similarly to (5.4) we find

$$W^{(2)}_{2S4S}\approx 1.5\cdot 10^{-4}\left(\frac{dP}{dS}\right)^{2}_{\text{W/cm}^2}. \tag{5.12}$$

Here we have assumed that the bandwidth of the laser radiation is small, $\Delta\omega\ll\Gamma_{4S}$. Then, taking a pulsed laser with power density of order 100 kW/cm^2, $\beta=0.054$ (1.4 MeV), and $L=5$ m, similarly to (5.5) we find the counting rate:

$$\dot{N}^{*}\approx 0.5\cdot\dot{N}_{\text{At}}.$$

This counting rate makes it possible to obtain something like one transition per laser pulse for $\dot{N}_{At}\sim 50$, pulse duration ~ 10 μsec, and repetition frequency ~ 4 kHz.

5.3. The $1S-2P$ one-photon transition

In spite of the quite large width of the $2P$ level, about 100 MHz, the precise measurement of this transition is interesting because it offers possibilities different from those described above in Sec. 4. The wavelength of the transition lies in the UV region, 121 nm, and even for colliding beams it is difficult to find a suitable laser. The problem is eased somewhat by the large absorption cross section at this transition:[19]

$$\sigma=256\pi\left(\frac{2}{3}\right)^{10}\frac{\alpha a_0^2\omega_0}{\Gamma}\approx 6.4\times 10^{-11}\ \text{cm}^2,\quad \Delta\omega\ll\Gamma. \tag{5.13}$$

It is therefore possible to use, for example, a cw He–Cd laser with wavelength 325 nm, and to work in the colliding beam mode with an antiproton energy of about 500 MeV ($\beta=0.756$).

The number of transitions per unit time in this case is obtained like (5.5) (see also Ref. 52), and in the laboratory frame it is

$$\dot{N}=\frac{(1+\beta)^2\gamma}{8\pi\beta}\cdot\frac{\sigma L}{\hbar\omega_0 c}\cdot\frac{dP}{dS}\cdot\dot{N}_{At}\approx 5.2\cdot 10^{-5}\times\frac{(1+\beta)^2\gamma}{\beta}\cdot L\left(\frac{dP}{dS}\right)_{\text{W/cm}^2}\cdot\dot{N}_{At},\ \text{sec}^{-1}. \tag{5.14}$$

Here the cross section σ in (5.13) is written in the rest frame of the atom, where it is expressed in terms of the atomic characteristics. For the same parameters as above ($L=5$ m, $\dot{N}_{At}=3\times 10^4$) and $dP/dS=1$ W/cm^2 we find

$$\dot{N}^{*}\approx 2\cdot 10^{3}\ \text{sec}^{-1}.$$

The power density we have chosen can be obtained using the He–Cd laser, and cw operation should provide good monochromaticity.

The detection scheme (Fig. 10) does not require the use of the cavities C, because the excited atoms make transitions into a short-lived $2P$ state. Their emission has the same features as in Sec. 5.1, i.e., it is shifted to the short-wavelength region relative to the laser radiation and is primarily forward-directed [Eqs. (5.6)–(5.8)]. Therefore, it is possible as before to record the integrated photon flux with energy discrimination and selection of coincidences with annihilation quanta. The estimates of the resolution, Eqs. (5.10) and (5.11), also remain valid, and here it is possible to expect a precision of $\delta\omega/\omega\sim 10^{-8}$.

Of course, the experiments discussed in this section do not exhaust all the possibilities of the optical spectroscopy of fast $\bar{H}^0$ atoms. In any case, it can be stated that all the spectroscopic measurements discussed for low-energy single antihydrogen atoms held in traps[4] can with some success be performed on a beam of fast atoms.

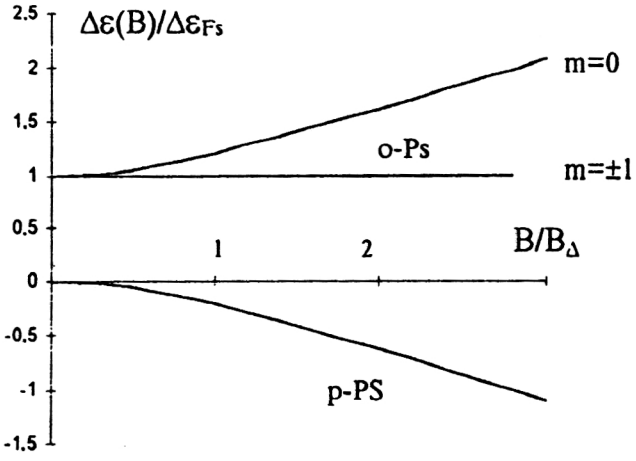

FIG. 11. Splitting of the ground state of positronium in a magnetic field.

6. EXPERIMENTS USING POSITRONIUM FLUXES

6.1. Positronium in a magnetic field

Positronium behaves in a magnetic field very much like a hydrogen atom (Sec. 4.4). A difference arises because the magnetic moments of the electron and positron, to the accuracy with which they are known at present, are equal in magnitude and opposite in sign. Therefore, in the ortho-state the total magnetic moment of positronium is zero, although the spin is one. In the para-state it is the reverse. As a result, in positronium there is no linear Zeeman effect (Fig. 11), and an ortho-level with $m=\pm 1$ does not react at all to the presence of a magnetic field B:[53]

$$\Delta\varepsilon_{\text{ortho}}(m=\pm 1)=\Delta\varepsilon_{FS}=\text{const},$$

$$\Delta\varepsilon_{\text{ortho}}(m=0)=\frac{\Delta\varepsilon_{FS}}{2}+\sqrt{\left(\frac{\Delta\varepsilon_{FS}}{2}\right)^2+(2\mu B)^2},$$

$$\Delta\varepsilon_{\text{para}}=\frac{\Delta\varepsilon_{FS}}{2}-\sqrt{\left(\frac{\Delta\varepsilon_{FS^2}}{2}+(2\mu B)^2\right.}. \tag{6.1}$$

Here $\Delta\varepsilon_{FS}$ is the difference of the ground-state energies (fine structure) of *o-Ps* and *p-Ps* (1.6), and μ is the electron (positron) magnetic moment.

The states of positronium mix in a magnetic field, similar to what occurs for atoms (Sec. IV A). Here, according to the above discussion, states of *o-Ps* with $m=\pm1$ remain unperturbed, and states of *o-Ps* with $m=0$ and *p-Ps* form a bound state, the dynamics of which is described[54] by the expressions in Sec. IV A. The level widths and lifetimes of *o-Ps* and *p-Ps* in a magnetic field are usually written as (see Refs. 53–55)

$$\Gamma'_o\equiv\tau_o^{-1}(B)=\frac{\Gamma_o+y^2\Gamma_p}{1+y^2},$$

$$\Gamma'_p\equiv\tau_p^{-1}(B)=\frac{\Gamma_p+y^2\Gamma_o}{1+y^2}, \tag{6.2}$$

$$y=(\sqrt{1+x^2}-1)/x\approx\begin{cases}x/2, & x\ll1,\\ 1-\dfrac{1}{x}, & x\gg1,\end{cases}$$

$$x=\frac{B}{B_\Delta},$$

$$B_\Delta=\frac{\Delta\varepsilon_{FS}}{4\mu}=3.62\ \text{T}. \tag{6.3}$$

Here $\Gamma_o=1/\tau_o$ and $\Gamma_p=1/\tau_p$ are the decay constants (level widths) and lifetimes of *p-Ps* and *o-Ps* in the free state (see Table II). It is easily verified that these expressions coincide with (4.10) for the substitution

$$\Omega_E\to2\mu B/\hbar\quad\Delta\omega\to\Delta\varepsilon_{FS}/\hbar,$$

$$\Gamma_d=\to\tau_o,\quad\Gamma_u\to\tau_p. \tag{6.4}$$

Then, accordingly,

$$\Gamma'_{d,u}=\tau_{p,o}^{-1}(B). \tag{6.5}$$

In a weak field $B\ll B_\Delta$ Eq. (6.2) for the lifetime becomes approximately

$$\tau_o^{-1}(B)\approx\tau_o^{-1}+\frac{x^2}{4}\tau_p^{-1},$$

$$\tau_p(B)\approx\tau_p. \tag{6.6}$$

Therefore, the lifetime $\tau_o(B)$ is slightly decreased, while $\tau_p(B)$ remains practically constant.

However, these expressions should not be viewed simply as the change of the lifetime of the two states of positronium (which, as a rule, is done in the studies cited). In fact, a mixed state of positronium in a magnetic field "lives" according to the law (4.9), (4.10). Therefore, the probability for decay of positronium in this mixed state into two or three gamma quanta is determined by the probability for positronium to stay in the *d* (para-) or *u* (ortho-) state (4.9).

The behavior of the flux of orthopositronium passing through the section with magnetic field can now be described completely.

We shall assume that this section is located rather far from the region of positronium generation (Fig. 5), so that at the entrance there is only the long-lived *o-Ps* component, the total flux of which is equal to $\dot N_{Ps}$. On the average, the positronium atoms at the entrance are divided with equal probability into *o*-Ps states with $m=0,\pm1$. Therefore, 2/3 of the flux corresponding to $m=\pm1$ states decays with constant τ_o, and the 1/3 going into the mixed state decays in accordance with (4.9). The flux at the exit of the segment is

$$\dot N_o(l)/\dot N_{Ps}=\frac{2}{3}\,e^{-\tau/\tau_o}+\frac{1}{3}\,P_u(\tau),$$

$$\dot N_p(l)/\dot N_{Ps}=\frac{1}{3}\,P_d(\tau), \tag{6.7}$$

where $\tau=l/v_0$ is the time to travel along the section of length l, and $P_{u,d}(\tau)$ are the values of the probabilities (4.9) at the exit of the segment [taking into account the substitution (6.4)]. It is convenient to write these expressions in terms of the parameters x and $y(x)$ [see Eq. (6.2)]:

$$\dot N_o(l)/\dot N_{Ps}=\frac{2}{3}\,e^{-\Gamma_o\tau}+\frac{1}{3(1+y^2)^2}\cdot(e^{-\Gamma'_o\tau}+y^4e^{-\Gamma'_p\tau}+2y^2e^{-\Gamma\tau}\cos\omega_x\tau),$$

$$\dot N_p(l)/\dot N_{Ps}=\frac{y^2}{3(1+y^2)^2}\cdot(e^{-\Gamma'_o\tau}+e^{-\Gamma'_p\tau}-2e^{-\Gamma\tau}\cdot\cos\omega_x\tau),$$

$$\omega_x=\sqrt{1+x^2}\,\frac{\Delta\varepsilon_{FS}}{\hbar},\quad\Gamma=\Gamma_o+\Gamma_p. \tag{6.8}$$

Oscillations of the *o-Ps* and *p-Ps* fluxes at the exit are noticeable if the lifetime is of order τ_p (Fig. 12). In particular, if the segment is sufficiently long that

$$\tau\sim\tau_o\gg\tau_p, \tag{6.9}$$

Eq. (6.8) in a weak field ($x\ll1$) can be written approximately as

$$\dot N_o(l)\approx\frac{\dot N_{Ps}}{3}(2e^{-\Gamma_o\tau}+e^{-\Gamma'_o\tau}),$$

$$\dot N_p(l)\approx\frac{\dot N_{Ps}}{12}\cdot\left(\frac{B}{B_\Delta}\right)^2\cdot e^{-\Gamma'_o\tau},\quad B\ll B_\Delta. \tag{6.10}$$

Therefore, at the exit of a long section with weak magnetic field there is a small fraction of parapositronium mixed with an attenuated flux of orthopositronium.

Just as important is the fact that in a magnetic field, 2/3 of the initial intensity (or half the total positronium flux generated by the storage device) decays according to the "usual" exponential law with constant Γ_o. In any case, the field at which the loss of positronium becomes significant is of order B_Δ.

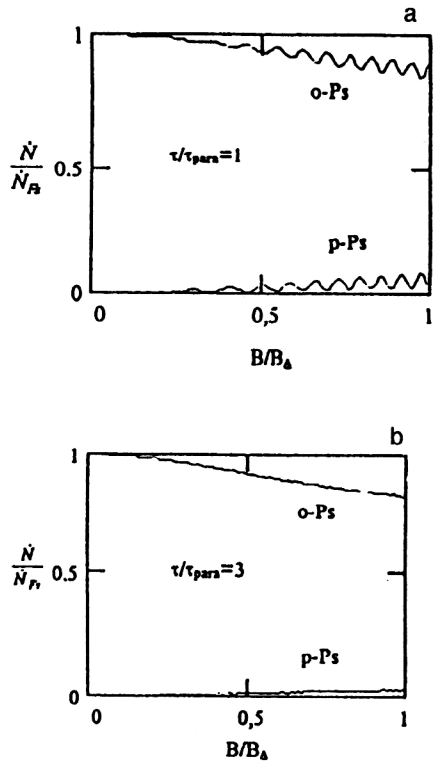

FIG. 12. Dependence of the intensity of (1) *o-Ps* and (2) *p-Ps* at the exit of the segment with magnetic field on the field strength. The time of flight is (a) $\tau=\tau_p$ and (b) $3\tau_p$. The notation is given in the text.

It is also useful to give the expressions for the total number of 3γ and 2γ annihilations per unit time on the segment with magnetic field. For this it is necessary to integrate over time the derivatives of the probability for positronium to survive in the ortho- or para-state. A special feature of the calculation of these derivatives should be noted. In the functions (4.9) or (6.8) describing the probability, it is not necessary to differentiate the factors $\cos \Omega t$ or $\cos \omega_x t$ in the last terms, because their derivatives give a probability flux from *o-Ps* to *p-Ps* and vice versa, while the number of annihilations per unit time comes from the derivatives of only the three exponentials. The integrals of the derivatives of the probability for the *o-Ps* state calculated in this manner give $\dot{N}^*_{3\gamma}$ for the number of 3γ annihilations, while for *p-Ps* they give $\dot{N}^*_{2\gamma}$ for the number of 2γ events. The resulting expressions are quite awkward, but nevertheless should be given here:

$$\dot{N}^*_{3\gamma}/\dot{N}_{Ps}=\frac{2}{3}(1-e^{-\Gamma_o\tau})+\frac{1}{3(1+y^2)}\cdot[1-e^{-\Gamma'_o\tau}+y^4(1-e^{-\Gamma'_p\tau})+y^2\cdot f(\tau)],$$

$$\dot{N}^*_{2\gamma}/\dot{N}_{Ps}=\frac{y^2}{3(1+y^2)}\cdot[2-e^{-\Gamma'_o\tau}-e^{-\Gamma'_p\tau}-f(\tau)],$$

$$f(\tau)=\frac{2\Gamma}{\Gamma^2+\omega_x^2}\cdot[\Gamma(1-e^{\Gamma\tau}\cdot\cos\omega_x\tau)+\omega_x e^{-\Gamma\tau}\cdot\sin\omega_x\tau]. \quad (6.11)$$

In the approximation of a long section (6.9) and weak field $y\ll 1$ we then find

$$\dot{N}^*_{3\gamma}=\dot{N}_{Ps}\left(1-\frac{2}{3}\cdot e^{-\Gamma_o\tau}-\frac{1}{3}\cdot e^{-\Gamma'_o\tau}\right),$$

$$\dot{N}^*_{2\gamma}=\frac{\dot{N}_{Ps}}{12}\left(\frac{B}{B_\Delta}\right)^2(2-e^{-\Gamma'_o\tau}). \quad (6.12)$$

The meaning of this expression is almost obvious: an *o-Ps* ($m=\pm 1$) state partially decays into 3γ with a decay constant Γ_o, and the upper mixed state also decays partially, but with a constant Γ'_o. The lower mixed state decays into 2γ partially with constant the Γ'_o and completely with the constant $\Gamma'_p\gg\tau^{-1}$, and this is the reason for the factor of two instead of one in the second expression. In this approximation the oscillatory terms vanish.

6.2. The lifetime of orthopositronium

The problem of the precise measurement of the *o-Ps* lifetime discussed in Sec. 1.2 requires an accuracy of better than 10^{-4} (see Table II). When a flux of orthopositronium is used it is possible to perform the classical version of the experiment: measurement of the dependence of the counting rate of triple coincidences (preferably with trajectory analysis) on the coordinate along the vacuum channel of positronium detection (Fig. 5, No. 8). For a positronium velocity of 10^{10} cm/sec the triple decay length is about 14 m, which for an angular spread of the flux of about 1.5 mrad (Table III) gives a flux size at the exit of about 20 mm.

The accuracy of measuring the lifetime in this version of the experiment [fitting the dependence $N(x)$ by an exponential law] is roughly

$$\varepsilon_\tau\leqslant\frac{e^k}{\sqrt{N_1}\ln N_1}+\frac{2\delta x}{L}, \quad (6.13)$$

where k is the ratio of the length of the detection channel and the decay length, N_1 is the number of counts collected at the channel entrance, and δx is the accuracy of measuring the coordinate. In this case an accuracy of $\varepsilon_\tau=10^{-5}$ for $k=3$ and $L=14$ m requires $N_1\sim 5\times 10^8$ and $\delta x\sim 0.15$ mm. It takes about 15 hours to collect this statistics for a flux of 10^4 sec^{-1}. Therefore, this level of accuracy appears to be attainable, and the possibility of performing the experiment in a vacuum makes it very attractive.

We note that the L_α photons arising in positronium formation can be used as start signals.

6.3. The lifetime of parapositronium

By using the mixing of the ortho- and para-states in a magnetic field, a flux enriched by parapositronium can be obtained at the exit of the segment containing the magnetic field. Then, by measuring the positronium decay with selection of *pair coincidences* in γ detection using the scheme of Sec. 6.2, it becomes possible to determine the *p-Ps* lifetime.

A well known difficulty is the short lifetime of *p-Ps*: at velocity 10^{10} cm/sec the triple decay length of *p-Ps* is only 3.75 cm. A possible solution of this problem is to record positronium absorption followed by annihilation in targets successively placed in the path of the positronium flux. In this case, it may be possible to localize the annihilation point with an accuracy of order 10 μm, which gives the main contribution to the measurement error:

$$\frac{\delta x}{L} \sim 3 \cdot 10^{-4}.$$

A fit to an exponential dependence allows the accuracy to be raised to 5×10^{-5}.

The second difficulty in this approach is the low intensity of the flux of the p-Ps component. However, this can be overcome by using, in addition to a magnetic field, excitation of transitions between positronium states in a varying electromagnetic field as in Secs. 4.2 and 4.4. The frequency of transitions between fine-structure levels (Fig. 11 and Table II) is of order 200 GHz, which corresponds [the Doppler shift (4.7) is small] to a wavelength of 1.5 mm. The detailed procedure was used in Ref. 29 to measure $\Delta\varepsilon_{FS}$.

Another method is an indirect one, where again state mixing and decrease of the o-Ps lifetime in a magnetic field (6.3) are used. This effect was also used in Ref. 26. In the case under discussion there is no possibility of having any start signal, and so it is impossible to use the same experimental setup as in Ref. 26. Instead, one can measure the dependence of the fluxes of 3γ and 2γ events on the magnetic field strength (the parameter y) and time-of-flight (energy variation), and then fit this dependence by the law (6.12), extracting the value of $\Gamma_o'(B)$ (6.2). When B and Γ_o are known, it is possible to calculate Γ_p. Obviously, a double fit can be performed here: $\dot{N}^*(B)$ can be fit by the law (6.12) and $\Gamma_o'(B)$ by the law (6.2). A level of precision of at least 10^{-5} can be counted on, because nearly all of the positronium flux is used in this setup.

6.4. Positronium spectroscopy

The experiments on the high-precision measurement of the positronium spectrum described in Sec. 1.2 (item 3) can also be performed using directed positronium fluxes. Owing to their high intensity and small velocity spread, a level of precision of at least 10^{-6} can be expected (an order of magnitude better than the Doppler spread; Table III). Both radiospectroscopic and laser-spectroscopic realizations of these experiments are possible. The latter may also allow measurements on two-photon transitions with cancellation of the Doppler broadening.

6.5. Searches for exotic decay channels and the "mirror world"

The version of the experiment to measure the o-Ps lifetime described in Sec. 6.2 can be extended to search for exotic decay channels, a short-lived boson, and the "mirror world" described in items 4–7 of Sec. I B.

The isolation of the decay channels in (1.7) requires an orthopositronium flux with the p-Ps component removed to the required level. For example, to measure the probability of o-Ps decay into 2γ at a level of 10^{-8} it is necessary to use a detection channel of length equal to more than 18 decay lengths of the para- component, which corresponds to only 70 cm for a velocity of 10^{10} cm/sec. Therefore, such an experiment can be performed under very clean conditions. The requirements on the purity for 4γ and higher decays are even easier to satisfy. The limit attained will then in practice be determined by the background conditions and counting errors in the coincidence recording.

The search for p-Ps decays of the type (1.8) is difficult owing to the background from o-Ps decays. Here it is possible to use the forced transition of positronium from the o-Ps to the p-Ps state described in Sec. 6.3, which offers special possibilities for extracting exotic events.

The search for short-lived bosons in o-Ps decays is also considerably easier in this case compared to the studies cited, owing to the purity of the experimental conditions and the high flux intensity. In particular, there is practically none of the intense background from positron annihilation in the target, which inevitably arises in the traditional setup where positronium is produced in the recombination of positrons stopped in the target with electrons of the target atoms. It is this background, and also the background from p-Ps decay, which is the main source of noise in the studies cited. Of course, it should be noted that for in-flight o-Ps decay the peak of the monochromatic gamma quanta is broadened compared to decay of positronium at rest. For example, two sharp peaks must be observed in the γ energy spectrum in the decay of stopped o-Ps according to the scheme (1.9): one from o-Ps decay into a boson and a γ, with γ energy

$$\varepsilon_1 = \left(m - \frac{m_b^2}{4m}\right)c^2, \tag{6.14}$$

and the other from decay of the boson into 2γ with

$$\varepsilon_2 = m_b c^2/2. \tag{6.15}$$

When these decays are recorded in an o-Ps flux with a single velocity, the peaks are shifted by an amount $\delta\varepsilon_\gamma \sim (\gamma - 1)\varepsilon_{1,2}$ and broadened, their width becoming

$$\Delta\varepsilon_\gamma \sim 2\beta(\varepsilon_\gamma)_{\max}.$$

This broadening makes detection of the peaks a bit more complicated, but the great improvement of the background conditions (in particular, the absence of the intense line from annihilation of positrons absorbed by the target in the traditional setup) more than compensates for this drawback.

Finally, the verification of the "mirror world" hypothesis reduces to measurement of the deviation of the distribution $N(x)$ of the number of decays along the channel length from an exponential law. Therefore, an experiment to measure the o-Ps lifetime in the setup described in Sec. 6.2 would simultaneously allow determination of the level of "runaway" positronium atoms.

CONCLUSIONS

Experiments on directed monochromatic atoms of antihydrogen and positronium reveal new possibilities for the experimental testing of the CPT theorem and quantum electrodynamics. In Table IV we give the accuracies of measuring the parameters of the fundamental particles and the simplest atoms which have been attained at present and which can be expected in the future on the basis of the estimates made above.

TABLE IV. Accuracies of the experimental values of the fundamental particle parameters.

Parameter	Accuracy	
	Attained	Expected
Difference of antiproton and positron electric charges, $\delta e/e$	$2\cdot10^{-5}$	$2\cdot10^{-9}$
The same for the electron, positron, proton, and antiproton, $\delta e/e$	$2\cdot10^{-5}$	$2\cdot10^{-8}$
Antiproton magnetic moment, $\delta\mu_a/\mu_a$	$3\cdot10^{-3}$	$2\cdot10^{-5}$
Difference of the proton and antiproton magnetic moments, $\delta\mu/\mu_N$	$3\cdot10^{-3}$	$1\cdot10^{-7}$
Hyperfine structure of the ground state of antihydrogen, $\delta\varepsilon/\varepsilon$	...	$3\cdot10^{-8}$
Hyperfine structure of the $2S_{1/2}$ level and Lamb shift of the $2P_{1/2}$ level, of antihydrogen, $\delta\varepsilon/\varepsilon$	...	$2\cdot10^{-5}$–$1\cdot10^{-6}$
Energry of $1S-2S$ transition in antihydrogen, $\delta\varepsilon/\varepsilon$	...	$1\cdot10^{-10}$

The author takes this opportunity to thank the following colleagues for fruitful discussions and collaboration: Yu. P. Gangrskiĭ, S. N. Gninenko, O. I. Kartavtsev, É. A. Kuraev, D. P. Mel', O. I. Meshkov, A. N. Skrinskiĭ, Yu. L. Sokolov, and M. Charlton.

The author would also like to thank W. Oelert for allowing him to read Ref. 3 in manuscript form, and T. A. Stepanova, L. V. Soboleva, and A. O. Sidorin for help in preparing this review. This work was performed with the support of the Russian Fund for Fundamental Research, Grant 96-02-17211

[1)]The recent suggestion[45] that the charge-exchange reaction be used to produce exotic atoms may lead to an increase of the flux intensity by several orders of magnitude compared to the version based on radiative recombination.

[2)]An accuracy of 1×10^{-12} has recently been reported (unpublished).

[1] G. I. Budker and A. N. Skrinskiĭ, Usp. Fiz. Nauk **124**, 561 (1978) [Sov. Phys. Usp. **21**, 277 (1978)].
[2] H. Herr, D. Moehl, and A. Winnacker, in *Physics at LEAR with Low-Energy Cooled Antiprotons* (Plenum Press, New York, 1984), p. 659.
[3] G. Baur, G. Boero, W. Oelert *et al.*, Phys. Lett. B **368**, 251 (1996).
[4] M. Charlton, J. Eades, D. Horvath *et al.*, Phys. Rep. **241**, 67 (1994).
[5] H. Poth, Appl. Phys. A **43**, 287 (1987).
[6] I. N. Meshkov, Fiz. Élem. Chastits At. Yadra **25**, 1487 (1994) [Sov. J. Part. Nucl. **25**, 631 (1994)].
[7] I. M. Meshkov and A. N. Skrinskiĭ, Preprint No. E9-95-130, JINR, Dubna (1995).
[8] N. F. Ramsey, Phys. Rev. **72**, 695 (1950); *Molecular Beams* (Clarendon Press, Oxford, 1950) [Russ transl., IL. Moscow 1960].
[9] J. W. Heberle, H. A. Reich, and P. Kusch, Phys. Rev. **101**, 612 (1956).
[10] Yu. L. Sokolov, Zh. Éksp. Teor. Fiz. **83**, 15 (1982) [Sov. Phys. JETP **56**, 7 (1982)].
[11] V. V. Parkhomchuk, in *Proc. of the Symp. on the Production and Investigation of Atomic Antimatter*, Karlsruhe, 1988, p. 315.
[12] H. Kopfermann, *Kernmomente* (Akademische Verlagsgesellschaft M.B.H., Frankfurt am Main, 1956) [Russian transl. from the German, Moscow, IL, 1960].
[13] I. N. Meshkov, Yad. Fiz. **59**, No. 8 (1996) [Phys. At. Nucl. **59**, No. 8 (1996)].
[14] *Review of Particle Properties*, Phys. Rev. D **50**, 1173 (1995).
[15] G. Gabrielse *et al.*, Phys. Rev. Lett. **74**, 35 (1995).
[16] A. Kreissl *et al.*, Z. Phys. C **37**, 557 (1988).
[17] R. Carosi *et al.*, Phys. Lett. B **237**, 303 (1990).
[18] L. D. Landau and E. M. Lifshitz, *Quantum Mechanics: Non-Relativistic Theory*, 3rd ed. (Pergamon Press, Oxford, 1977) [Russ. original, Nauka, Moscow, 1974].
[19] V. B. Berestetskiĭ, E. M. Lifshitz, and L. P. Pitaevskiĭ, *Relativistic Quantum Theory* (Pergamon Press, Oxford, 1971) [Russ. original, Nauka, Moscow, 1968].
[20] R. P. Feynman, *Quantum Electrodynamics* (Benjamin, New York, 1962) [Russ. transl., Mir, Moscow, 1964].
[21] (a)G. S. Adkins, A. A. Salakuddin, and K. E. Schalm, Phys. Ref. A **45**, 7774 (1992); (b) P. Labelle, G. P. Lepage, and U. Magnea, Phys. Rev. Lett. **72**, 2006 (1994).
[22] C. I. Westbrook, D. W. Gidley, R. S. Conti, and A. Rich, Phys. Lett. A **40**, 5489 (1972).
[23] C. I. Westbrook, D. W. Gidley, R. S. Conti, and A. Rich, Phys. Rev. Lett. **58**, 1328 (1987).
[24] J. S. Nico, D. W. Gidley, A. Rich, and P. W. Zitzewitz, Phys. Rev. Lett. **65**, 1334 (1990).
[25] S. Asai, S. Orito, and N. Shinohara, Phys. Lett. B **357**, 475 (1995).
[26] A. H. 'Al-Ramadhan and D. W. Gidley, Phys. Rev. Lett. **72**, 1632 (1994).
[27] É. A. Kuraev, G. V. Kukhto, and Z. K. Silagadze, Yad. Fiz. **51**, 1638 (1990) [Sov. J. Nucl. Phys. **51**, 1036 (1990)]; Preprint No. 89-154, Institute of Nuclear Physics, Siberian Division, Russian Academy of Sciences (1989) [in Russian].
[28] A. I. Mil'shtein and I. B. Khriplovich, Zh. Éksp. Teor. Fiz. **106**, 689 (1994) [JETP **79**, 379 (1994)].
[29] S. Chu, A. P. Mills, and J. H. Hall, Phys. Rev. Lett. **52**, 1689 (1984).
[30] K. Danzmann, M. S. Fee, and S. Chu, Phys. Rev. A **39**, 6072 (1989).
[31] M. W. Ritter, P. O. Egan, V. W. Hughes, and K. A. Woodle, Phys. Rev. A **30**, 1331 (1984).
[32] S. Hatamian, R. S. Conti, and A. Rich, Phys. Rev. Lett. **58**, 1833 (1987).
[33] D. W. Gidley, J. S. Nico, and M. Scalsey, Phys. Rev. Lett. **66**, 1302 (1991).
[34] S. Adachi, M. Chiba, T. Hirose *et al.*, Phys. Rev. Lett. **65**, 2634 (1990).
[35] U. Amaldi, G. Carboni, B. Jonson, and J. Thun, Phys. Lett. B **153**, 444 (1985).
[36] (a) S. Orito, K. Yoshimura, T. Haga *et al.*, Phys. Rev. Lett. **63**, 597 (1989); (b) M. Tsuchiaki, S. Orito, T. Yoshida, and M. Minowa, Phys. Lett. B**236**, 81 (1990).
[37] M. V. Akopyan, G. S. Atoyan, S. N. Gninenko, and V. V. Sukhov, Phys. Lett. B **272**, 443 (1991).
[38] S. Asai, K. Shigekuni, T. Sanuki, and S. Orito, Phys. Lett. B **323**, 90 (1994).
[39] I. Yu. Kobzarev, L. B. Okun', and I. Ya. Pomeranchuk, Yad. Fiz. **3**, 1154 (1966) [Sov. J. Nucl. Phys. **3**, 837 (1966)].
[40] S. L. Glashow, Phys. Lett. B **167**, 35 (1986).
[41] S. N. Gninenko, Phys. Lett. B **326**, 317 (1994).
[42] A. S. Artamonov, Ya. S. Derbenev, and E. L. Saldin, Part. Accel. **23**, 73 (1988).
[43] Ya. S. Derbenev, private communication (1995).
[44] M. Charlton and G. Lariccia, Hyperfine Ints. **76**, 97 (1993).
[45] O. I. Kartavtsev and I. N. Meshkov, J. Phys. **29**, 4303 (1996).
[46] V. M. Galitskiĭ, B. M. Karnakov, and V. I. Kogan, in *Problems in Quantum Mechanics* [in Russian] (Nauka, Moscow, 1981).
[47] L. B. Okun, *Leptons and Quarks*, 2nd ed. (North-Holland, Amsterdam, 1984) [Russ. original, Nauka, Moscow, 1990, p91].
[48] N. B. Delone, *Interaction of Laser Radiation With Matter* [in Russian] (Nauka, Moscow, 1989, pp. 42-45); N. B. Delone and M. V. Fedorov, Proc. Lebedev Institute **115**, 42 (1980).
[49] F. Schmidt-Kaler *et al.*, Phys. Rev. A **51**, 2789 (1995).
[50] L. S. Vasilenko, V. P. Chebotaev, and A. B. Shishaev, JETP Lett. **12**, 113 (1970); V. S. Letokhov and V. P. Chebotaev, *Nonlinear Laser Spectroscopy With Superhigh Resolution* [in Russian] (Nauka, Moscow, 1990).
[51] H. A. Bethe and E. E. Salpeter, *Quantum Mechanics of One- and Two-Electron Atoms* (Academic Press, New York, 1957) [Russ. transl., Fizmatgiz, Moscow, 1960, p. 418, Table 15].
[52] L. D. Landau and E. M. Lifshitz, *The Classical Theory of Fields*, 4th English ed. (Pergamon Press, Oxford, 1975) [Russ. original, Nauka, Moscow, 1967].
[53] V. I. Gol'danskiĭ, *The Physical Chemistry of the Positron and Positronium* [in Russian] (Nauka, Moscow, 1968).
[54] O. Halpern, Phys. Rev. **94**, 904 (1954).
[55] A. Rich, Rev. Mod. Phys. **53**, 127 (1981).

Translated by Patricia A. Millard